444 | September 1984

SCHRIFTENREIHE SCHIFFBAU

P. Oltmann und S.D. Sharma

Simulation of Combined Engine and Rudder Maneuvers using an Improved Model of Hull-Propeller-Rudder Interactions

TUHH
Technische Universität Hamburg-Harburg

Simulation of Combined Engine and Rudder Maneuvers using an improved Model of Hull-Propeller-Rudder Interactions

Peter Oltmann, Som D. Sharma, Hamburg, Technische Universität Hamburg-Harburg, 1984

Schriftenreihe Schiffbau
Schwarzenbergstraße 95c
D-21073 Hamburg

http://www.tuhh.de/vss

Institut für Schiffbau der Universität Hamburg

SIMULATION OF COMBINED ENGINE AND RUDDER MANEUVERS USING AN IMPROVED MODEL OF HULL-PROPELLER-RUDDER INTERACTIONS

by

P. Oltmann and S.D. Sharma

Prepared for the
Fifteenth ONR Symposium on Naval Hydrodynamics
Hamburg, 3 - 7 September 1984

September 1984 Bericht Nr. 444

CONTENTS

CONTENTS (Contd.)

Simulation of Combined Engine and Rudder Maneuvers Using an Improved Model of Hull-Propeller-Rudder Interactions

Peter Oltmann and Som D. Sharma

ABSTRACT

Digital simulations of combined engine and rudder maneuvers are presented for two representative ship types, namely a single-screw tanker and a twin-screw center-rudder container carrier. The hydrodynamic coefficients occurring in the dynamical equations have been derived from special four-quadrant force measurements on ship models in the captive mode and partially validated by trajectory measurements in the free-running mode, both by means of the Computerized Planar Motion Carriage at the Hamburg Ship Model Basin (HSVA). Contrary to previous versions, the new mathematical model is not restricted to small changes of initial forward speed and can be applied even to maneuvers involving speed reversal. For this purpose, it was found to be necessary to adopt a compact physically motivated rather than a formal mathematical series approximation of the hydrodynamic forces as functions of motion variables and to explicitly account for the three-way hull-propeller-rudder interactions in the system.

NOMENCLATURE

Abbreviations

CPMC	Computerized planar motion carriage
CPRM	Constant propeller rate, model cond.
CPRS	Constant propeller rate, ship cond.
CSRS	Constant steam rate, ship condition
HSVA	*Hamburgische Schiffbau-Versuchsanstalt* (Hamburg Ship Model Basin)
ITTC	International Towing Tank Conference
MSPP	Model self-propulsion point
SSPP	Ship self-propulsion point

Symbols

A_R	Total rudder area
A_{RP}	Rudder area swept by propeller race
A_f, A_b	Turbine torque parameters, Sect. 2.3
A_o	Propeller disk area
a, b	Turbine torque parameters, Sect. 2.3
a_0, a_7, a_8, a_9	Parameters associated with hull cross flow drag coefficient, Sect. 2.2.4
B_f, B_b	Turbine torque parameters, Sect. 2.3
C_{CFD}	Coefficient of local cross flow drag
C_{DR}	Rudder drag coefficient, Sect. 2.2.7
C_{DR}^o	Rudder drag coefficient at $u_P/\bar{u}_R = 0$
C_F	Frictional drag coefficient
C_{LR}	Rudder lift coefficient, Sect. 2.2.7
C_{LR}^o	Rudder lift coefficient at $u_P/\bar{u}_R = 0$
C_Q^*	Propeller torque coeff., Sect. 2.2.6
C_T^*	Propeller thrust coeff., Sect. 2.2.6
c, d, e, k, c', d', e'	Parameters associated with lifting forces on the hull, Sect. 2.2.3
c_P	Circumferential velocity of propeller blade at 0.7 radius
D	Diameter of propeller
d	Distance between propeller disk and quarter mean chord of rudder
F	Force in general
G	Center of gravity
g	Acceleration due to gravity
I_{zz}	Moment of inertia about z-axis
I_{EP}	Effective moment of inertia about propeller axis
k	Correction or amplification factor in general
k_{HR}, k_{PR}	Interaction factors, Sect. 2.2.7
k_{LR}, k_{DR}	Amplification factors, Sect. 2.2.7
L	Length between perpendiculars
l	Half-length
m	Mass
N	Hydrodynamic moment about z-axis
n	Rate of revolutions of propeller
0	Coordinate origin fixed in the body
Q	Propeller torque
Q_E	Engine torque
q_F	Engine fuel rate
q_S	Turbine steam rate
R	Turning radius
R_T	Total hull resistance

Peter Oltmann, Hamburgische Schiffbau-Versuchsanstalt, Postfach 600929, 2000 Hamburg 60, FR Germany
Som D. Sharma, Institut für Schiffbau der Universität Hamburg, Lämmersieth 90, 2000 Hamburg 60, FRG

r	Rate of turn about z-axis (yaw rate)
s	Distance along track
T	Draft
T	Period of zigzag maneuver
T	Propeller thrust
t	Thrust deduction fraction
t	Time
U	Along-track velocity of O
U_O	Initial value of U
u_A	Axial velocity induced by propeller
$u_{A\infty}$	Asymptotic value of u_A at infinity
u,v	Components of U along x,y-axes
u_P	Speed of advance of propeller
$\bar{u}_R$	Mean flow velocity past rudder
w	Taylor wake fraction
X,Y	Hydrodynamic forces along x,y-axes
x,y,z	Coordinate axes fixed in the body
x_G,y_G,z_G	Coordinates of center of gravity
x_o,y_o,z_o	Coordinates of O in an earth-fixed system, Fig. 1
α_o	Overshoot angle in zigzag maneuver
β	Drift angle
β_R	Local drift angle at rudder
γ	Yaw rate angle, Sect. 2.2.3
δ	Rudder angle
δ_e	Effective rudder angle
δ_m	Max. value of δ in zigzag maneuver
ε	Propeller advance angle, Sect. 2.2.6
ρ	Mass density of water
τ	Characteristic times of zigzag maneuver, Fig. 2
τ_a	Time to attain switching value ψ_s
τ_b	Time to check yaw rate r
τ_c	Time for counterturn
τ_r	Reach time
τ_L	Time lag of steering gear
ψ	Heading angle
ψ_s	Switching value of ψ in zigzag man.

Notes

As far as possible, ITTC standard symbols and the SI units have been used. Several special rules have been adopted or devised for achieving greater clarity and for generating compound symbols in a systematic and meaningful way. Vertical and italic type has been consistently used (except for Greek letters) to distinguish between abbreviations and numerical variables.

Subscript abbreviations H,P,R and I,L,C have been used singly and multiply to indicate that the subscripted quantity is associated with the hull, propeller and rudder or the ideal-fluid, lifting and cross-flow effects respectively. Subscript variables u,v,r etc. have been used to identify corresponding coefficients in a polynomial expansion for the subscripted quantity. Other subscripts and superscripts have been used in the conventional manner.

All time-independent system parameters have been ultimately reduced to nondimensional numbers, see Table 3. In many cases this has been done according to the socalled bis-system, i.e. by multiplying the (") superscripted quantity by the necessary powers of certain fundamental units of mass, length and time, namely m, L and $\sqrt{L/g}$ respectively.

1. INTRODUCTION

Both the demand and the capability of simulating ship maneuvers on digital computers have grown dramatically during the last twenty years, fed by the increasing need of ship operators to define and document maneuverability on the one hand and the ready availability of ever more efficient computers on the other. A specially strong incentive has also come from the now widespread use of real-time ship simulators for the training of nautical personnel.

Any algorithm for the simulation of ship maneuvers must incorporate as a key element an explicit or implicit mathematical model of the hydrodynamics of the maneuvering vessel. For lack of a matured hydrodynamic theory dictating an all-embracing standard format, the number of heuristic mathematical models in use has also proliferated. However, it is fair to say that the three dominant models on the market are due to Abkowitz (1964), Norrbin (1970), and the Mathematical Model Group of the Society of Naval Architects of Japan (JMMG for short) as reported by Ogawa and Kasai (1978).

The highly formal and systematic Abkowitz model treats the hull-water interface essentially as a black box and is based on the notion of a maneuver being a small perturbation of an equilibrium state of steady forward motion at designed speed. Nevertheless, it has proven very successful for the simulation of arbitrary rudder maneuvers at constant engine setting as documented by the pioneering work of Strøm-Tejsen and Chislett (1966) followed by many others including our own group, cf. Oltmann and Wolff (1979) and Wolff (1981). In a modified form it has even been applied to engine maneuvers, by Crane (1973) and Eda (1974) for example, despite the fact that such maneuvers can hardly be considered "small" perturbations of an equilibrium state.

The Norrbin model is less formal, more physically motivated and very broadly conceived, even including approximate corrections for shallow and restricted water effects, cf. Berlekom and Goddard (1972) and Norrbin (1978).

The JMMG model is quite heuristic and pays special attention to hull-propeller-rudder interactions, but is also restricted to maneuvers retaining considerable forward speed. It works alright for rudder maneuvers as exemplified by Matsumoto and Suemitsu (1981). Moreover, a great amount of additional effort has been undertaken in Japan recently to cover also stopping maneuvers, as documented by Tanaka and Miyata (1977), Yoshimura and Nomoto (1978), Fujino et al. (1979) and summarized in the latest Report of the Maneuverability Committee of the 17th ITTC (1984).

The principal purpose of this paper is to

present an alternative mathematical model suitable for the digital simulation of combined engine and rudder maneuvers for a wide range of surface ships. The core of this model is a rather new scheme for the mathematical approximation of the complex hydrodynamic forces generated in response to the motion of a maneuvering hull and to the operation of its primary control organs (rudder and screw propeller). This new approach, necessitated by the inadequate performance of previous models in the vicinity of zero forward speed, has evolved gradually over the last five years. Portions of it have already appeared in print, cf. Sharma and Zimmermann (1981) and Sharma (1982a). However, a comprehensive description of the total model accompanied by examples of simulated maneuvers is being published here for the first time. The main advantages claimed for the new model are applicability to forward and backward motion, explicit accounting of the three-way hull-propeller-rudder interaction, corrections for major scale effects, and the modeling of engine characteristics up to and even beyond speed reversal.

2. MATHEMATICAL MODEL

2.1. Dynamical Equations

The equations of motion of a surface ship maneuvering in the horizontal plane with three degress of freedom (namely surge, sway and yaw) can be written down as usual in the following form (see also Fig. 1):

$$\dot{x}_o = u\cos\psi - v\sin\psi \tag{1}$$

$$\dot{y}_o = u\sin\psi + v\cos\psi \tag{2}$$

$$\dot{\psi} = r \tag{3}$$

$$(\dot{u} - vr - r^2 x_G)\, m = X \tag{4}$$

$$(\dot{v} + ur + \dot{r}x_G)\, m = Y \tag{5}$$

$$\dot{r} I_{zz} + (\dot{v} + ur)\, x_G m = N \tag{6}$$

The basic assumptions at this stage are that the ship may be treated as a rigid body and that the "vertical" motions of heave, pitch and roll are either negligible or at least decoupled from the "horizontal" motions of surge, sway and yaw. The external force-couple X,Y,N acting on the ship will in general comprise applied forces as well as complex hydrodynamic and aerodynamic reactions to the time history of the ship's motion and appropriate control actions. The various competing models for the simulation of ship maneuvers currently in vogue differ mainly in which forces they take into account and how these are explicitly related to the numerous variables and parameters of the system.

Consistent with the limited scope of this paper we shall consider here exclusively hydrodynamic response forces of the quasisteady type. These will be discussed in due detail in the following section. However, there are two particular aspects of these forces, pertaining to the general format and number of the dynamical equations, which are better anticipated here.

Firstly, these forces are found to depend in a significant way on the rudder angle δ and the propeller rate n. The question therefore arises whether the variables δ,n can be simply treated as control input or whether additional dynamic equations must be introduced accounting for the inertia of the steering gear and the propulsion plant. The compromise attitude adopted here is that the rudder angle may be considered as a direct control variable subject to simple constraints whereas the following dynamic equation is optionally added to achieve greater flexibility and realism in the simulation of engine maneuvers:

$$2\pi \dot{n} I_{EP} = Q_E - Q \tag{7}$$

Under this option the propeller torque Q depends mainly on longitudinal velocity u and propeller rate n, while the engine torque Q_E depends essentially on propeller rate n and some suitable engine input such as the fuel rate q_F. Hence we end up with seven state variables x_o,y_o,ψ,u,v,r,n and two control variables δ,q_F.

Secondly, the hydrodynamic response forces contain the usual linear acceleration terms dictated by classical hydrodynamic theory. Hence a simple reshuffling of Equations (4-7) is required to get all the acceleration terms and only these on the left hand sides. When the linear acceleration coupling still persisting in Equations (5-6) is also eliminated by solving algebraically for $\dot{v},\dot{r}$ the canonical format of the dynamical equations emerges expressing the time rate of change of state as a vector function of state variables, control variables and time-independent parameters. Trajectory simulation for any given initial state and control input is then easily accomplished on a digital computer using any standard algorithm for the numerical integration of a system of ordinary differential equations.

2.2. Hydrodynamic Forces

2.2.1. General Outline

It will be helpful to outline the basic philosophy behind our present model of the hydrodynamic response forces before going into its unavoidably complex details. As already stated, our main motivation for developing this new approach was the operational demand for simulation of combined engine and rudder maneuvers often employed in shiphandling and in emergency situations like an impending collision. Hence the primary requirement on the mathematical description of the forces was that it must not break down in the proximity of hull or propeller speed reversal, as is unfortunately the case with most conventional models utilizing longitudinal velocity u and propeller rate n as reference quantities for scaling the forces. In view of the overriding importance of this objective, certain other effects have been ignored or simplified for the time being.

Thus the ship is taken to be maneuvering in an otherwise undisturbed, homogeneous, isotropic

environment on horizontally unbounded waters of uniform depth. So the forces need not depend explicitly on the position variables x_0, y_0, ψ or the water depth, effectively decoupling the kinematic Equations (1-3) from the remaining dynamic Equations (4-7). Moreover, possible time history effects are neglected so that, except for certain linear acceleration terms dictated by potential theory, the response forces X,Y,N,Q can be supposed to depend only on the instantaneous values of just five dynamic variables u,v,r,n,δ. Within the domain of validity delimited by these putative premises the model has been kept perfectly general. This has been achieved by introducing the following four angles (see Nomenclature):

$$\beta = \arctan(-v/u) \tag{8}$$

$$\gamma = \arctan(rl/u) \tag{9}$$

$$\delta_e = \delta + \beta_R, \quad \beta_R = \arctan(-v_R/\bar{u}_R) \tag{10}$$

$$\varepsilon = \arctan(u_P/c_P) \tag{11}$$

to express all possible relative magnitudes of the five variables u,v,r,δ,n, and by insisting that the force descriptions chosen remain valid in all four quadrants of each of these four angles. By way of comparison it may be noted that for simulating simple rudder maneuvers the range of validity required in terms of these angles is only about one tenth as large.

In order to satisfy this fourfold four-quadrant requirement it was found to be necessary to depart in three major respects from the previously used direct input-output models which blindly but elegantly expressed X,Y,N as formal polynomials of u,v,r,δ. Firstly, the forces had to be partly decomposed into contributions associated with the system elements hull, propeller and rudder on the one hand and with the physical mechanisms labeled ideal fluid, hull lifting and cross-flow effects on the other:

$$X = X_I + X_{HL} - R_T + X_P + X_R \tag{12}$$

$$Y = Y_I + Y_{HL} + Y_{HC} + Y_P + Y_R \tag{13}$$

$$N = N_I + N_{HL} + N_{HC} + N_P + N_R \tag{14}$$

Secondly, a number of intermediate variables had to be introduced, mainly to account for interaction effects such as wake, thrust deduction, slipstream, flow rectification etc. between the three system elements. Thirdly, a wider set of physically motivated functions than mere polynomials had to be invoked to achieve reasonable accuracy without sacrificing compactness.

This four-quadrant model has so far been identified and partly validated by means of suitable model experiments in the captive and free-running modes for four representative ship types of which only two will be discussed in this paper, namely a single-screw tanker (see Table 1 and Fig. 3) and a twin-screw center-rudder container carrier (see Table 2 and Fig. 4). It needs to be said that such four-quadrant experiments (specially in the yaw rate angle γ) were rendered feasible only by the availability of our Computerized Planar Motion Carriage (CPMC) described previously at these Symposia, cf. Grim et al. (1976) and Oltmann et al. (1980). To our knowledge no comparable set of complete four-quadrant experiments has been elsewhere reported in the literature.

Although our model experiments covered all four quadrants completely and uniformly, see Sharma and Zimmermann (1981), the present analysis has been significantly simplified by taking advantage of the nearly perfect port-and-starboard symmetry inherent in every ship. The only hydrodynamically relevant asymmetry stems from the rotation in the slipstream of a single-screw propeller. We have isolated its effect by comparing the measured forces for corresponding odd and even values of β,γ,δ and lumped it up in just two terms, namely Y_P, N_P. The remaining terms in Eq. (12-14), practically all of which are directly or indirectly affected by the action of the propeller, thus refer to a symmetrized system. Consequently, the forces are either exactly symmetric (X) or anti-symmetric (Y,N) functions of the angles β,γ,δ, and need to be displayed in the first two quadrants only.

2.2.2. Ideal Fluid Effects

According to a famous theorem of potential theory the hydrodynamic forces generated by the irrotational flow of an otherwise undisturbed, unbounded ideal fluid in response to the general motion of an arbitrarily shaped rigid body can be explained in terms of an "added inertia" tensor consisting of a symmetric 6×6 matrix of coefficients determined by the body form alone. An often cited classical derivation of this result can be found in Lamb (1932, p. 160 ff.) and a modern marine hydrodynamic version in Newman (1977, p. 135 ff.). A particularly perspicuous rendering of the complete expressions for these forces on a body moving with six degrees of freedom was given in the present nomenclature by Imlay (1961).

If we ignore the wavemaking at the free surface - a reasonable simplification for low Froude numbers in the present context - the horizontally maneuvering surface ship becomes equivalent to (the lower half of) a mirror-symmetric double-body moving in an unbounded fluid with three degrees of freedom only. The relevant portion of the added inertia tensor then reduces to the following 3×3 matrix:

$$\begin{bmatrix} -X_{\dot{u}} & -X_{\dot{v}} & -X_{\dot{r}} \\ -Y_{\dot{u}} & -Y_{\dot{v}} & -Y_{\dot{r}} \\ -N_{\dot{u}} & -N_{\dot{v}} & -N_{\dot{r}} \end{bmatrix}$$

The symbols are chosen to reflect the immediate interpretation of the individual elements of the inertia tensor as acceleration derivatives, i.e. as factors of proportionality for the forces and moments with which the fluid resists the accelerations of the body. The port and starboard symmetry inherent in almost every hull form entails the further simplifications:

$$X_{\dot{v}} = Y_{\dot{u}} = 0, \quad X_{\dot{r}} = N_{\dot{v}} = 0 \tag{15}$$

The near fore-and-aft symmetry, also usually prevailing, implies that the remaining coupling coefficients are small compared to the direct effects:

$$Y_{\dot{r}} = N_{\dot{v}} << X_{\dot{u}}, Y_{\dot{v}}, N_{\dot{r}} \quad (16)$$

and the slenderness of the hull ($B,T<<L$) ensures that the longitudinal effects are small compared to the transverse effects:

$$X_{\dot{u}} << Y_{\dot{v}}, N_{\dot{r}} \quad (17)$$

A somewhat surprising result of this theory is that although every single element of the inertia tensor may be considered an acceleration derivative the complete final expressions for the forces also contain terms involving velocities. Accordingly, our model comprises the following expressions for the forces associated with "ideal fluid" effects:

$$X_I = X_{\dot{u}}\dot{u} + X_{vr}vr + X_{rr}r^2 + X_{vv}v^2 \quad (18)$$

$$Y_I = Y_{\dot{v}}\dot{v} + X_{\dot{u}}ur + Y_{\dot{r}}\dot{r} \quad (19)$$

$$N_I = N_{\dot{r}}\dot{r} + N_{\dot{v}}(\dot{v} + ur) + (Y_{\dot{v}} - X_{\dot{u}})uv \quad (20)$$

It is worth noting that these expressions deviate in certain details from the strict potential theory. The latter would require

$$X_{vr} = -Y_{\dot{v}},\ X_{rr} = -Y_{\dot{r}} = -N_{\dot{v}},\ X_{vv} = 0 \quad (21)$$

However, since our goal is not to estimate the true ideal fluid effects - amenable to computation only - but to simulate a part of the real effects observed in model experiment after the pattern of potential theory, this slight generalization comprising eight distinct form-dependent parameters instead of only four allowed by the strict theory seems justified.

The nondimensionalized numerical values of these eight parameters for our tanker form, as identified by suitable experiments, are documented in Table 3. It will be seen that the only serious departure from the mandates of the theory is the significant nonequality of the derivatives X_{vr} and $-Y_{\dot{v}}$. Of particular interest in the context of maneuvering are the side force and yaw moment in response to the velocities u,v,r in steady motion. The ideal fluid contributions to these forces according to the above equations are depicted in nondimensional coefficient form as functions of drift angle and yaw rate angle by the long dashed curves in Figs. 5 and 6 respectively, in relation to the other contributions explained in subsequent sections. It will be noted from Fig. 5 (bottom) that the term $(Y_{\dot{v}} - X_{\dot{u}})uv$, sometimes called the Munk moment, plays a dominant role in maneuvering dynamics.

2.2.3. Hull Lifting Effects

Although a displacement hull - unlike a hydrofoil or rudder - is not primarily designed to generate circulation and lift, it nevertheless acts like a slender lifting body in inclined flow. The resulting side force and yaw moment in response to the combined longitudinal and transverse motion play a crucial role in maneuvering. Our model of these lifting effects is based on three simplified principles of airfoil theory, see for instance Prandtl and Tietjens (1934, p. 144 ff.). First, the lift F_L is proportional to the underwater lateral area, the stagnation pressure of the effective inflow, and the sine of twice the effective angle of attack; it acts normal to the inflow. Second, the lift is accompanied by a parasitic induced drag F_D proportional to the square of the lift and acting parallel to the inflow. Third, the yaw moment is obtained by multiplying the resulting side force with an effective lever representing the longitudinal distance x_F of the center of action of the lifting forces from the coordinate origin. Under these assumptions the lifting effects can be correctly approximated over four quadrants of the angle of attack by a minimum of three empirical constants for a given hull shape and flow configuration.

Thus the effect of drift (u and v) can be quantified in a straightforward manner by the three equations:

$$F_L = c\,LT\,\frac{\rho}{2}(u^2+v^2)\cos\beta\sin\beta \quad (22)$$

$$F_D = d\,F_L\cos\beta\sin\beta \quad (23)$$

$$x_F = -\frac{e}{c}L\,\mathrm{sgn}u \quad (24)$$

incorporating the coefficients c,d,e as three nondimensional, positive hull-form parameters. The factor $\mathrm{sgn}u$ accounts for the fact that the hydrodynamic trailing edge responsible for the generation of lift through the Kutta condition lies at the stern for $u > 0$ and at the stem for $u < 0$. The equivalent force-couple resolved along body coordinates becomes:

$$X = F_L\sin\beta - F_D\cos\beta \quad (25)$$

$$Y = F_L\cos\beta + F_D\sin\beta \quad (26)$$

$$N = -\frac{e}{c}LY\,\mathrm{sgn}u \quad (27)$$

The situation in yaw (u and r) is analogous but slightly more complicated. Here the steady motion of the hull along a circular arc gives rise to a centripetal lift, somewhat comparable to the action of a cambered body in steady translation. In any case, an additional constant k is desirable to average the locally variable transverse velocity and define an effective angle of attack at the active trailing edge:

$$\gamma^* = \arctan\left(\frac{krl\,\mathrm{sgn}u}{u}\right) \quad (28)$$

which differs subtly from the purely kinematic yaw rate angle γ used to identify the relative magnitudes of u and r. The lifting effect of yaw is then expressed by equations analogous to (22-27) substituting $krl\,\mathrm{sgn}u$ for $-v$, γ^* for β, and three new form parameters c',d',e' for c,d,e.

As an example, the numerical values of these seven parameters as determined from suit-

able model experiments for our tanker hull are listed in Table 3. Their contributions to side force and yaw moment in response to drift and yaw are plotted in Figs. 5 and 6 as the short-dashed curves for the sake of comparison with the two other effects. Attention is called to the following features. First, in our model the ideal fluid and lifting effects together constitute what are ordinarily called "linear" terms in the expansions for side force and yaw moment about the equilibrium point $v,r = 0$. Second, single analytical expressions could serve in four quadrants only because we made the lift proportional to the sine of twice the angle of attack instead of just the angle of attack as is common practice. Third, a constant position for the center of lift (somewhere in the active after body) makes sense only because we have segregated other effects, especially the Munk moment.

The final step required for completing the description of hull lifting effects is the treatment of a combined drift and yaw motion. This synthesis has been effected in a heuristic way by a linear combination of weighted transverse velocities, making sure that the limiting cases come out alright. The final expressions, now directly in terms of the velocities u,v,r, are as follows:

$$X_{HL} = \frac{\rho}{2} LT \frac{u(c'krl\,\mathrm{sgn}u - cv)}{\sqrt{u^2+(krl\,\mathrm{sgn}u - v)^2}} \times \left\{ (krl\,\mathrm{sgn}u - v) - \frac{u^2(d'krl\,\mathrm{sgn}u - dv)}{u^2+(krl\,\mathrm{sgn}u - v)^2} \right\} \quad (29)$$

$$Y_{HL} = \frac{\rho}{2} LT \frac{u^2(c'krl\,\mathrm{sgn}u - cv)}{\sqrt{u^2+(krl\,\mathrm{sgn}u - v)^2}} \times \left\{ 1 + \frac{(d'krl\,\mathrm{sgn}u - dv)(krl\,\mathrm{sgn}u - v)}{u^2+(krl\,\mathrm{sgn}u - v)^2} \right\} \quad (30)$$

$$N_{HL} = -\frac{\rho}{2} L^2T \frac{u|u|(e'krl\,\mathrm{sgn}u - ev)}{\sqrt{u^2+(krl\,\mathrm{sgn}u - v)^2}} \times \left\{ 1 + \frac{(d'krl\,\mathrm{sgn}u - dv)(krl\,\mathrm{sgn}u - v)}{u^2+(krl\,\mathrm{sgn}u - v)^2} \right\} \quad (31)$$

We note parenthetically that the use of the above expressions beyond speed reversal ($u=0$) with parameters c,d,e etc. identified for forward motion ($u>0$) is tantamount to ignoring the minor fore-and-aft asymmetry of the hull, which is generally permissible. However, if higher accuracy is required for reverse motion ($u<0$) only the numerical values of the parameters need be slightly changed, retaining the general format of these expressions.

2.2.4. Hull Cross-Flow Effects

The essentially nonlinear cross-flow forces on the hull in response to its transverse motion are relatively large, for the hull is purposely designed to have a low longitudinal and a high transverse resistance. They are modeled here according to a simple strip theory along the lines of Norrbin (1978). The elementary side force dY_{HC} on a hull element of length dx is assumed to be proportional to the stagnation pressure of the local transverse flow velocity $(v+rx)$, the local draft $T(x)$ and the local coefficient of cross-flow drag $C_{CFD}(x)$. So the total side force and yaw moment can be expressed as follows:

$$Y_{HC} = -\frac{\rho}{2} \int_{-l_a}^{l_f} T(x) C_{CFD}(x) (v+rx)|v+rx|\,dx \quad (32)$$

$$N_{HC} = -\frac{\rho}{2} \int_{-l_a}^{l_f} T(x) C_{CFD}(x) (v+rx)|v+rx|\,x\,dx \quad (33)$$

These integrals can be solved in closed form using suitable analytical approximations (e.g. polynomials) for the functions $T(x)$ and $C_{CFD}(x)$.

In special cases (e.g. asymmetric profile, inclined keel, trim or heel) it may be useful to allow for different lengths of afterbody and forebody l_a,l_f as well as for a variable draft $T(x)$. In most cases, however, the following simplifications prevail:

$$l_a = l_f = l, \qquad T(x) = \text{const} = T \quad (34)$$

As regards the local variation of cross-flow drag coefficient, it has been found convenient to use a high-order four-term polynomial such as

$$C_{CFD}(x) = a_0 + a_7(x/l)^7 + a_8(x/l)^8 + a_9(x/l)^9 \quad (35)$$

which is well suited to approximate a fairly constant value over the parallel midbody, rising substantially toward the ends with a certain amount of asymmetry (to account for the propeller or a bulb for instance), as illustrated in Fig. 8 for our tanker form. The reason for using just four terms is that the four unknown coefficients a_0,a_7,a_8,a_9 can be fitted exactly to the four measured values of side force and yaw moment coefficients at zero forward speed ($\beta = 90^0$ and $\gamma = 90^0$) where pure cross-flow effects can be observed without interference from ideal-fluid or lifting effects.

Note that the above analytical expressions are not used for determining the cross-flow forces *a priori* but in effect for interpolating them continuously over the four quadrants of drift angle and yaw rate angle (as well as their combinations) on the basis of their observed values at zero longitudinal motion and their theoretical values (namely zero) at zero transverse motion ($\beta = \gamma = 0$). As shown by the dash-dotted curves in Figs. 5 and 6 the relative importance of cross-flow forces increases steadily with decreasing longitudinal motion and is maximum at $\beta = 90^0$ and $\gamma = 90^0$. The dominant effects are a resistive side force in

response to drift and a resistive yaw moment in response to yaw rate. The rather weak coupling manifested as side force in response to yaw rate and yaw moment in response to drift arises, of course, from the small fore-and-aft asymmetry of the hull.

The strictly nonlinear mechanism by which simultaneous drift and yaw unite to generate a combined side force and yaw moment is automatically taken care of by the above formulas. This is illustrated in nondimensional coefficient form in Fig. 7 for all possible combinations of transverse velocity v and yaw rate r. In addition, the contribution of each term of the polynomial $C_{CFD}(x)$ is individually shown. It is seen that the even terms a_0,a_8 (responsible for the direct effects) dominate, while the odd terms a_7,a_9 (responsible for the coupling) largely annihilate each other. It has been found that the total effects are quite insensitive to the polynomial degree chosen for representing $C_{CFD}(x)$. For instance, an alternative calculation based on the same experimental data but a third degree polynomial (a_0, a_1,a_2,a_3) for interpolation yielded a somewhat unrealistic curve for the associated local drag coefficient but practically the same integrated cross forces for all transverse motions.

2.2.5. Hull Resistance

The ordinary hull resistance to pure longitudinal motion is measured in a routine model test and extrapolated to full-scale in the conventional manner by decomposing the nondimensional coefficient of total resistance:

$$C_T = 2R_T/\rho S u^2 \tag{36}$$

into viscous and wave components:

$$C_T(R_n,F_n) = (1+k)\,C_F(R_n) + C_W(F_n) \tag{37}$$

subject to Reynolds and Froude scaling respectively, and using the 1957 ITTC correlation line to calculate the Reynolds-number dependent frictional coefficient C_F. In the simulation algorithm, however, a suitable polynomial fit is preferred to avoid numerical problems with the term $C_F(R_n)$ near zero forward speed:

$$R_T(u) = R_{Tu}u + R_{Tu|u|}u|u| + R_{Tuuu}u^3 \tag{38}$$

The nondimensionalized polynomial coefficients for the tanker form are included in Table 3. Obviously, the numerical values must be different for the model condition and the ship condition owing to the scale effect on viscous resistance. Strictly speaking, the values given were determined for forward motion. However, the formula applies also to backward motion without serious error. If higher precision is desired, a separate set of coefficients may be used for negative speeds or the expression modified to include a small even term in u.

2.2.6. Propeller Forces

Accurate modeling of the propeller forces is of utmost importance for the correct simulation of engine maneuvers, specially those involving thrust, torque and speed reversal, such as the crashback. The forces of primary interest are, of course, the thrust T, and the torque Q if the additional dynamical Equation (7) is also used. Obviously, the conventional representation of propeller characteristics in terms of advance coefficient J and thrust and torque coefficients K_T,K_Q is unsatisfactory because J is ambiguous for negative speeds and everything breaks down at n=0:

$$J = u_P/nD, \quad K_T = T/\rho n^2 D^4, \quad K_Q = Q/\rho n^2 D^5 \tag{39}$$

The proper way to cover all possible combinations of axial and rotational motion is to introduce an advance angle ε and new force coefficients C_T^*, C_Q^* in terms of axial and circumferential blade velocities u_P,c_P at a significant radius:

$$\varepsilon = \arctan(u_P/c_P), \quad c_P = 0.7\pi n D \tag{40}$$

$$C_T^* = 2T/\rho A_o(u_P^2 + c_P^2) \tag{41}$$

$$C_Q^* = 2Q/\rho A_o D(u_P^2 + c_P^2) \tag{42}$$

For any given propeller the functions $C_T^*(\varepsilon)$, $C_Q^*(\varepsilon)$ can be determined by experiment and smoothly interpolated in four quadrants by finite Fourier series, as was first demonstrated for the Wageningen B-Screw Series by van Lammeren et al. (1969). However, this mathematically elegant approximation is not very efficient, for as many as 2 × 40 Fourier coefficients are required to achieve adequate accuracy, cf. also Laudan (1974). We therefore advocate a more flexible approach pursuing the principle of parsimony. Our simulation algorithm currently employs a composite approximation. Over the short range of advance angles between the bollard-pull condition (ε=0) and the zero-thrust condition ($\varepsilon \approx 20^0$) where a high percentage accuracy is desired we recommend either tabular interpolation in the open-water diagram or a low-order algebraic or trigonometric polynomial fit. Over the remaining interval one can safely use the following compact functions:

$$C_T^*(\varepsilon) = A_T \cos\varepsilon|\cos\varepsilon| - B_T \sin\varepsilon|\sin\varepsilon| \tag{43}$$

$$C_Q^*(\varepsilon) = A_Q \cos\varepsilon|\cos\varepsilon| - B_Q \sin\varepsilon|\sin\varepsilon| \tag{44}$$

custom-tailored to roughly reproduce the global characteristics with just two parameters each.

By way of illustration, the relevant expressions for our tanker propeller are listed in Table 3 and plotted in Fig. 9. It will be noted that no more than five parameters are used for each force. An additional set may be optionally inserted if higher accuracy in backward motion $-180^0 < \varepsilon < 0^0$ is needed.

Such economy is mandatory also in view of future extensions to account for the effect of transverse motions, which has been systematically investigated by our group, cf. Laudan (1977), but not yet incorporated into the simulation model.

Whereas in the previous Sections the com-

plex interactions between the elements hull, propeller and rudder were only implicitly included in so far as the model identification rested on forces measured on the total system, we must now account explicitly for wake and thrust deduction to adapt the open-water characteristics to the behind-hull condition. This is done by the conventional rules:

$$u_P = (1-w)u, \quad X_P = (1-t)T \tag{45}$$

Although our four-quadrant experiments in the behind-hull condition have revealed complicated variations of wake fraction w and thrust-deduction fraction t with the advance angle ε, pending further analysis we have chosen to employ just two distinct values each for forward and backward motion. However, we do apply an important scale-effect correction in extrapolating the wake from model to ship according to the ITTC 1978/84 standard procedures for single and twin screws. For example, the wake fraction of our tanker decreases by about 30% from model to full-scale, see Table 3.

Finally, the side force and yaw moment generated directly and indirectly by the hydrodynamic asymmetry inherent in a single-screw ship must be modeled, cf. Saunders (1957, p. 496 ff.) and Mandel (1967, p. 332 ff.). As discussed in detail elsewhere, this effect is rather weak and sensitive in steady forward motion, cf. Oltmann et al. (1980), but quite strong and consequential in stopping or reversing when the inverted propeller slipstream hits the hull, cf. Sharma (1982b). For the present purpose it has been found sufficient to postulate a linear dependence on thrust:

$$Y_P = Y_{PT}T, \quad N_P = N_{PT}T \tag{46}$$

with the factors of proportionality assuming different values for forward and backward thrust and motion. Typical numbers are given in Table 3 for the tanker. It is almost needless to add that the terms Y_P, N_P vanish for any symmetric twin-screw arrangement as in our Fig. 4.

2.2.7. Rudder Forces

The rudder being the key element in ship maneuvering deserves the most careful consideration. Our model of the rudder forces is conceptually straightforward but by no means practically so. Essentially, we treat the rudder as a symmetric control surface fully characterized by its empirical lift and drag coefficients in two quadrants, e.g. see Fig. 10. These coefficients, derived from measurements in the behind-ship condition, represent the total system response to rudder application and not merely the forces acting on the (movable part of the) rudder itself. Since the movement of the model rudder is often constrained to about $\pm 40^0$ the gaps may have to be filled by reference to relevant data on similar rudders investigated in the freestream, e.g. see Thieme (1962). Unlike the smooth lifting characteristics of the slender hull, the coefficients of the rudder by virtue of its higher aspect ratio exhibit typical discontinuities reflecting stall. Hence they must be approximated by multiple piecewise analytical functions or simple tabular interpolation, cf. Table 3.

The practical difficulties in the identification as well as subsequent simulation of rudder forces lie in the determination of the highly variable, complex flow conditions at the rudder. Here the interaction effects of the hull and the propeller come into full play. Let us first consider the relatively simple case of a rudder operating outside the slipstream, as on our container carrier (Fig. 4). Then only the hull influence needs to be taken into account, say through an average wake fraction w_R and a flow rectification factor k_{HR}, so that the effective longitudinal and transverse velocities at the rudder become simply:

$$u_R = (1-w_R)u, \quad v_R = (v+rx_R)k_{HR} \tag{47}$$

This implies an effective angle of attack δ_e equal to the sum of the geometric rudder angle δ and the local drift angle β_R, see Eq. (10), leading to the following expressions for the effective rudder forces resolved along hull coordinates:

$$X_R = \frac{\rho}{2} A_R(u_R^2 + v_R^2)(C_{LR}\sin\beta_R - C_{DR}\cos\beta_R) \tag{48}$$

$$Y_R = \frac{\rho}{2} A_R(u_R^2 + v_R^2)(C_{LR}\cos\beta_R + C_{DR}\sin\beta_R) \tag{49}$$

$$N_R = Y_R x_R \tag{50}$$

However, if the rudder is wholly or partially immersed in the slipstream, as in the case of our tanker (Fig. 3), the additional influence of the propeller must be considered. This requires a tedious procedure involving several steps, of which only a simplified version is given here omitting a few *ad hoc* rules for treating marginal cases. First of all, the asymptotic axial velocity increment in the slipstream at infinity can be estimated from elementary momentum theory:

$$u_{A\infty} = (\mathrm{sgn}u)\sqrt{u_P^2 + (\mathrm{sgn}u)\ 2T/\rho A_o} - u_P \tag{51}$$

Application of a factor k_{PR}, depending only on the relative distance d/D of the rudder from the propeller disk after Gutsche (1955), then yields the axial flow velocity at the location of the rudder:

$$u_{RP} = u_P + \{(k_{PR} - \tfrac{1}{2})\mathrm{sgn}u + \tfrac{1}{2}\}\, u_{A\infty} \tag{52}$$

For estimating the area A_{RP} of the rudder subjected to this velocity, the slipstream diameter D_{RP} in way of the rudder can be calculated from the condition of continuity:

$$D_{RP}^2 u_{RP} = D^2(u_P + \tfrac{1}{2} u_{A\infty}) \tag{53}$$

An average longitudinal flow velocity $\bar{u}_R$ at the rudder can then be defined by:

$$\bar{u}_R^2 = \{A_{RP}u_{RP}^2 + (A_R - A_{RP})\, u_R^2\}/A_R \tag{54}$$

Other investigators have, in effect, reported that the influence of the propeller on the rudder is adequately accounted for by simply sub-

stituting $\bar{u}_R$ for u_R in Eq. (48-49), cf. Thulin (1974) or Landgraf and Müller (1975). However, our experience indicates a significant residual dependence on thrust loading, which can be expressed as a linear variation with the velocity ratio $u_P/\bar{u}_R$ within the range (0,1):

$$C_{LR} = (1 + k_{LR}u_P/\bar{u}_R)\, C^o_{LR} \qquad (55)$$

$$C_{DR} = (1 + k_{DR}u_P/\bar{u}_R)\, C^o_{DR} \qquad (56)$$

$$N_R = (1 - k_{NR}u_P/\bar{u}_R)\, Y_R x_R \qquad (57)$$

This effect probably arises from the nonuniform velocity distribution over the rudder, the rotation in the slipstream and the flaplike action of the rudder behind the hull. In any case, three additional factors k_{LR}, k_{DR}, k_{NR} suffice to take care of this phenomenon, see Table 3 for the tanker. Moreover, the rudder characteristics must now refer to some particular value of the velocity ratio $u_P/\bar{u}_R$, for instance zero in Table 3 or one-half in Fig. 10.

Finally, it is worth emphasizing that corrections for scale effects enter into this algorithm directly through the wake fractions and indirectly through the thrust loading which varies to match the hull resistance.

2.3. Machinery Characteristics

Obviously the dynamics of the ship's steering gear and propulsion plant have a direct influence on the time history of its maneuvers. It is realized that for certain special tasks such as the finetuning of an autopilot an accurate and detailed knowledge of the transfer function between commanded helm and executed rudder angle is required. However, for a computation of the ship's trajectory in substantial turning or checking maneuvers we think it reasonable to treat the helm angle as a direct input variable subject to some simple constraints, such as a prescribed time lag τ_L and given upper bounds on executable rudder angle $|\delta|$ and rudder rate $|\dot{\delta}|$, the standard values being 35 deg and 2.3 deg/s respectively.

As regards the propulsion plant, our simulation model provides two independent options. Most marine engines nowadays have automatic controllers which maintain a constant rate of revolutions in face of varying load (within limits) and trigger a predetermined temporal pattern of RPM change in response to an engine command from the bridge. On some ships the RPM can be explicitly controlled from the bridge. In all these cases we treat RPM as a direct input variable subject to suitable constraints.

On the other hand, there are several situations where the RPM should be treated as an output variable subject to the dynamic equilibrium of the rotating propeller shaft. This occurs when the engine is being operated at constant fuel rate or when the RPM controller is unable to maintain a steady rate against increasing load for lack of power reserve or when the RPM controller is intentionally overridden in an emergency maneuver such as the crashback. For handling these situations our simulation model has an additional (optional) dynamic equation (see Sect. 2.1.), which presupposes that the engine torque can be expressed as a quasisteady function of fuel rate and RPM. This socalled torque characteristic depends crucially on engine type and is very different for diesel engines and steam turbines. For the latter we adapted a fairly general bilinear formula given by Geisler and Siemer (1974):

$$q^*_s \geq 0: \quad Q^*_E = A_f\left(\frac{q^*_s - a}{1-a}\right)(1-n^*) + B_f\left(\frac{q^*_s - b}{1-b}\right)n^* \qquad (58)$$

$$q^*_s < 0: \quad Q^*_E = A_b\left(\frac{q^*_s + a}{1-a}\right)(1+n^*) - B_b\left(\frac{q^*_s + b}{1-b}\right)n^* \qquad (59)$$

Here q^*, Q^*_E and n^* denote nondimensional relative steam rate, engine torque and RPM respectively, each expressed as a fraction of its full rated value. Typical values of the nondimensional parameters a,b and A_f, B_f (for the main turbine) and A_b, B_b (for the astern turbine, formally implied by a "negative" steam rate) are given in Table 3. It so happens that the two prototype ships treated in this paper both had steam turbines.

It should be noted that in free-running tests with ship models in a towing tank the propulsion plant is almost invariably an electric motor with sufficient power reserve and simple RPM control. Hence the model maneuvers are normally executed at constant propeller rate irrespective of the torque characteristics of the prototype. However, devices comprising torque feedback and a programmable micro-computer are now available for driving a model propeller in accordance with a specified engine characteristic.

3. SAMPLE RESULTS

3.1. Preamble

The usefulness of the foregoing mathematical model will now be examined by dint of sample results obtained for two quite different ships, namely a single-screw tanker and a twin-screw center-rudder container carrier. Their main dimensions are listed in Tables 1 and 2, and the hull lines are displayed in Figs. 3 and 4 respectively. Not only do they represent the two most important classes of merchant ships afloat today, but they are also significantly different in their hull form parameters and propeller-rudder configurations, so as to be ideally suited as test cases for the present purpose.

For each ship three series of definitive maneuvers have been simulated, namely zigzags, turning circles, and crashbacks with and without rudder application. These are generally considered adequate for identifying the turning, checking and stopping capabilities in a comprehensive manner.

Almost every maneuver has been simulated under two distinct conditions, briefly designated CPRM and CSRS. The first condition implies a constant propeller rate corresponding to the model self-propulsion point (MSPP) for the approach speed and no scale effect corrections for model resistance and wake. This computation

is thus equivalent to a direct Froude scaling of free-running maneuvers in a model tank, where the electric drive can hold a constant RPM by virtue of its power reserve. The second condition implies the extrapolation of resistance and wake from model to full-scale according to the standard ITTC procedure and a constant fuel or steam rate corresponding to the ship self-propulsion point (SSPP) at the approach speed. The rate of revolutions then varies during the maneuver depending upon the torque characteristics of the engine and the propeller. For the crashback maneuvers, of course, the steam flux is not held constant but diverted to the astern turbine in the shortest admissible time up to the highest permissible value.

For the convenience of readers and rivals who may wish to reproduce our results or scrutinize our simulation scheme the requisite set of system parameters, besides the pertinent principal particulars, is listed for one of the ships (the tanker) in Table 3. For the same reason an adequate amount of simulation output is presented digitally in Tables 4 and 5 in addition to the customary graphs. It is not claimed, however, that the numbers reported are significant to the last listed digit. A systematic sensitivity survey has not yet been attempted for the subject model.

3.2. Tanker

The maneuvering hydrodynamic interest of this tanker hinges on its relatively tiny propeller operating at a high thrust loading behind a full-bodied hull so that the hull-propeller-rudder interactions are pretty pronounced and the scale effects are rather large. All maneuver simulations reported here start with a steady approach speed of 15 kn at either 98.8 RPM (MSPP) or 85.8 RPM (SSPP), the latter corresponding to 76% rated power or 79% rated steam flux.

Let us consider the zigzag maneuvers first. A partial time history of the standard $20^0/20^0$ zigzags is plotted in Fig. 11 and selected output of two systematic series of zigzags is shown in Fig. 12, consult also Fig. 2 for definitions. Since the results marked CPRM have been previously validated by reference to trajectories of a freely maneuvering model in the CPMC tracking mode, the interest here lies in the comparison of CPRM and CSRS. Clearly, the differences are rather small, partly because of the self-correcting feedback strategy inherent in a zigzag maneuver and partly because the hydrodynamic scale effect and the differing engine characteristics tend to countervail each other. In general, the response times, overshoots, turning rates and transfers are slightly lower under ship conditions.

Turning now to the hard-starboard turning circle time-histories in Fig. 13 and trajectories in Fig. 14, we observe a marked difference between CPRM and CSRS, see also Table 5 for a complete overview of turning characteristics. As might have been expected the final speeds and turning rates are lower for the ship, but it is not self-evident why the drift angle should be larger and the turning circle tighter. The real value of a simulation algorithm lies in revealing counter-intuitive behavior.

The most interesting results, however, were obtained for the crashbacks, simulated by diverting the full rated steam flux to the astern turbine within 27 seconds, without and with simultaneous rudder application, see Figs. 15 and 16. Three outstanding features are noticed. First, there is a striking tendency to turn to starboard in stopping even with rudder held amidships. Second, simultaneous hard starboard rudder hardly affects the time history but markedly shortens the advance. Third, by far the shortest advance is achieved by rudder hard to starboard while steaming full ahead!

3.3. Container Carrier

Our container carrier is a bit beamy but slender and has an out-of-the-rut twin-screw center-rudder configuration (Table 2 and Fig. 4). The simulations reported here all start with a steady approach speed of 16 kn either at 85.8 RPM (MSPP) or at 74.7 RPM (SSPP) corresponding to only 30% rated power or 28% rated steam flux. This modest speed with an enormous power reserve was originally chosen for the sake of correlation with some full-scale maneuver data that happened to be accessible.

The zigzag and turning circle maneuvers are shown in Figs. 17 to 20 in a manner exactly analogous to Figs. 11 to 14 for the tanker. Surprisingly, despite the conspicuous differences in hull form and propeller-rudder arrangement, the zigzag characteristics are almost indistinguishable. The turning circles, of course, show significant differences. The container carrier attains the final steady state much sooner, has no bias to starboard, a turning radius twice as large, and reverts almost exactly to original track after a complete circle. The relation of CPRM to CSRS is the same as for the tanker.

The most dramatic difference from the tanker, however, is observed in the fantastic stopping capability of the overpowered container carrier, compare Figs. 21-22 vs. 15-16. Rudder application further reduces both the stopping time and the stopping distance. In marked contrast to the tanker a hard turning circle produces the same advance as a crashback straight on the track. The shortest advance is achieved by a radical combined engine and rudder maneuver.

The authors trust this pilot probe into the vast space of combined engine and rudder maneuvers now opened to study by simulation shall serve to demonstrate the power and utility of the proposed four-quadrant model. Yet it can only be a tentative prototype likely to undergo many modifications in the foreseeable future.

ACKNOWLEDGMENT

This paper is an offshoot of a long-term research project concerning the safety of ships against collisions, sponsored by the German Research Association (*Deutsche Forschungsgemeinschaft*) within the framework of a Special Research Pool for Marine Technology (*Sonderforschungsbereich 98 "Schiffstechnik und Schiffbau"*) at Hamburg and Hanover.

REFERENCES

Abkowitz, M.A. (1964): Lectures on ship hydrodynamics - Steering and maneuverability. Hydro- and Aerodynamics Laboratory, Lyngby/Denmark, Report Hy-5.

Berlekom, W.B.; Goddard, T.A. (1972): Maneuvering of large tankers. Transactions SNAME, Vol. 80, pp. 264-298.

Crane, C.L. (1973): Maneuvering safety of large tankers: Stopping, turning and speed selection. Transactions SNAME, Vol. 81, pp. 213-242.

Eda, H. (1974): Digital simulation analysis of maneuvering performance. Proc. 10th ONR Symposium on Naval Hydrodynamics, Cambridge MA/USA, pp. 181-205.

Fujino, M.; Kirita, A.; Nishihata, A. (1979): On the manoeuvrability of ships while stopping by adverse rotation of propeller - 2nd Report (in Japanese). Journal of Kansai Society of Naval Architects of Japan, Vol. 173, pp. 45-55.

Geisler, O.; Siemer, G. (1974): Dynamische Belastung von Schiffsdampfturbinenanlagen bei Umsteuermanövern. Schiff & Hafen, Vol. 26, pp. 213-218.

Grim, O.; Oltmann, P.; Sharma, S.D.; Wolff, K. (1976): CPMC - A novel facility for planar motion testing of ship models. Proc. 11th ONR Symposium on Naval Hydrodynamics, London/UK, pp. 115-131.

Gutsche, F. (1955): Die Induktion der axialen Strahlzusatzgeschwindigkeit in der Umgebung der Schraubenebene, Schiffstechnik, Vol. 3, pp. 31-33.

Imlay, F.H. (1961): The complete expressions for "added mass" of a rigid body moving in an ideal fluid. Hydro. Lab. R & D Report 1528, David Taylor Model Basin, Carderock MD/USA.

Lamb, H. (1952): Hydrodynamics. Cambridge University Press (Reprint of Sixth Edition, 1932), Cambridge/UK.

Lammeren, W.P.A. van; Manen, J. D. van; Oosterveld, M.W.C. (1969): The Wageningen B-Screw Series. Transactions SNAME, Vol. 77, pp. 269-317.

Landgraf, J.; Müller, E. (1975): Ruder im Schraubenstrahl. Jahrbuch STG, Vol. 69, pp. 361-371.

Laudan, J. (1974): Propellerkräfte und -momente beim geradlinigen Stoppmanöver. HSVA-Report No. F4/74, Hamburg.

Laudan, J. (1977): Zweiquadrantenmessungen bei Schräganströmung hinter einem Schiffsmodell. HSVA-Report No. 1508, Hamburg.

Mandel, P. (1967): Ship Maneuvering and Control. Chapter VIII, Principles of Naval Architecture, SNAME, New York NY/USA, pp. 463-606.

Matsumoto, N.; Suemitsu, K. (1981): Experimental prediction method of manoeuvring performance of ships and ocean structures. Nippon Kokan Technical Report No. 32, Tokyo/Japan.

Newman, J.N. (1977): Marine Hydrodynamics. The M.I.T. Press, Cambridge MA/USA.

Norrbin, N. (1970): Theory and observations on the use of a mathematical model for ship maneuvering in deep and confined waters. Proc. 8th ONR Symposium on Naval Hydrodynamics, Pasadena CA/USA, pp. 807-904.

Norrbin, N. (1978): A method for the prediction of the maneuvering lane of a ship in a channel of varying width. Proc. Symp. "Aspects of Navigability of Constraint Waterways, Including Harbour Entrances", Delft/Holland, Vol. 3, Paper 22.

Ogawa, A.; Kasai, H. (1978): On the mathematical model of manoeuvring motion of ships. International Shipbuilding Progress, Vol. 25, pp. 306-319.

Oltmann, P.; Wolff, K. (1979): Vergleichende Untersuchung über das Manövrierverhalten des MARINER-Standardschiffes. Institut für Schiffbau, Hamburg, Report No. 385.

Oltmann, P.; Sharma, S.D.; Wolff, K. (1980): An investigation of certain scale effects in maneuvering tests with ship models. Proc. 13th ONR Symposium on Naval Hydrodynamics, Tokyo/Japan, pp. 779-801.

Prandtl, L.; Tietjens, O.G. (1957): Applied Hydro- and Aeromechanics. Dover Publications, New York NY/USA (Reprint of 1934 Edition).

Saunders, H.E. (1957): Hydrodynamics in Ship Design, Vol. I. SNAME, New York NY/USA.

Sharma, S.D. (1982a): Schrägschlepp- und Drehversuche in vier Quadranten - Teil 2. Schiff & Hafen, Vol. 34, pp. 219-222.

Sharma, S.D. (1982b): Bemerkungen über die Steuerwirkung von Propellern. Jahrbuch STG, Vol. 76, pp. 111-117.

Sharma, S.D.; Zimmermann, B. (1981): Schrägschlepp- und Drehversuche in vier Quadranten - Teil 1. Schiff & Hafen, Vol. 33, pp. 123-125.

Smitt, L.W.; Chislett, M.S. (1974): Large amplitude PMM tests and maneuvering predictions for a Mariner class vessel. Proc. 10th ONR Symposium on Naval Hydrodynamics, Cambridge MA/USA, pp. 131-157.

Strøm-Tejsen, J.; Chislett, M.S. (1966): A model testing technique and method of analysis for the prediction of steering and maneuvering qualities of surface ships. Proc. 6th ONR Symposium on Naval Hydrodynamics, Washington DC/USA, pp. 317-381.

Tanaka, M.; Miyata, H. (1977): Simulation program for maneuverability of ships and its application. Japan Shipbuilding & Marine Engineering, Vol. 11, No. 4, pp. 5-14.

Thieme, H. (1962): Zur Formgebung von Schiffsrudern. Jahrbuch STG, Vol. 56, pp. 381-426.

Thulin, S.A.R. (1974): Discussion to Smitt and Chislett (1974). Proc. 10th ONR Symposium on Naval Hydrodynamics, Cambridge MA/USA, pp. 153-156.

Wolff, K. (1981): Ermittlung der Manövriereigenschaften fünf repräsentativer Schiffstypen mit Hilfe von CPMC-Modellversuchen. Institut für Schiffbau, Hamburg, Report No. 412.

Yoshimura, Y.; Nomoto, K. (1978): Modeling of manoeuvring behaviour of ships with a propeller idling, boosting and reversing (in Japanese). Journal of The Society of Naval Architects of Japan, Vol. 144, pp. 57-69.

Note: Tables 1 to 5, Figures 1 to 22 and an Addendum follow.

Table 1 Main dimensions of the tanker (HSVA Model 2507, Scale 1 : 35)

Length between perpendiculars	290.000	m
Length of waterline	296.446	m
Beam	47.500	m
Draft forward	16.196	m
Draft aft	15.964	m
Block coefficient	0.805	
LCB fwd of midship section	7.243	m
Radius of gyration (z-axis)	66.360	m
Number of propellers	1	
Diameter	7.910	m
Pitch ratio	0.745	
Expanded area ratio	0.600	
Number of blades	5	
Sense of rotation	right	
Number of rudders	1	
Rudder area	73.500	m^2
Chord length	7.150	m
Aspect ratio	1.438	
Turbine plant:		
Rated power	20 608.0	kW
Rated speed.	95.0	RPM
Effective moment of inertia about propeller axis	766.2	tm^2

Table 2 Main dimensions of the container carrier (HSVA Model 2657, Scale 1 : 34)

Length between perpendiculars	273.000	m
Length of waterline	279.351	m
Beam	32.200	m
Draft forward	12.200	m
Draft aft	12.200	m
Block coefficient	0.611	
LCB aft of midship section	5.435	m
Radius of gyration (z-axis)	61.880	m
Number of propellers	2	
Diameter	6.150	m
Pitch ratio	1.200	
Expanded area ratio	0.860	
Number of blades	5	
Sense of rotation	outward	
Number of rudders	1	
Rudder area	59.350	m^2
Chord length	5.850	m
Aspect ratio	1.734	
Turbine plant;		
Rated power	2 × 29 233.4	kW
Rated speed	136.0	RPM
Effective moment of inertia about propeller axis	2 × 948.1	tm^2

Table 3 System parameters of the tanker for maneuver simulation

Hydrodynamic Characteristics

Ideal Fluid Effects:

$X''_{\dot{u}} = -0.0737$ $X''_{vr} = 0.6482$
$X''_{rr} = 0.0423$ $X''_{vv} = -0.0261$
$Y''_{\dot{v}} = -0.7810$ $Y''_{\dot{r}} = -0.0488$
$N''_{\dot{r}} = -0.0394$ $N''_{\dot{v}} = -0.0357$

Hull Cross-Flow Effects:

$a_0 = 0.207$ $a_7 = 5.310$
$a_8 = 3.218$ $a_9 = -6.732$

Hull Lifting Effects:

$c = 0.240$ $c' = 0.500$
$d = 1.000$ $d' = 1.000$
$e = 0.064$ $e' = 0.100$
$k = 0.400$

Hull Resistance:

	(Model)	(Ship)
R''_{Tu}	0.00162	0.00109
$R''_{Tu\|u\|}$	0.04034	0.02364
R''_{Tuuu}	0.07659	0.03594

Propeller Coefficients:

$0^0 < \varepsilon < 21^0$: $C^*_T = -0.833 + 1.020 \cos\varepsilon - 0.332 \sin\varepsilon$

$10C^*_Q = -1.171 + 1.378 \cos\varepsilon - 0.235 \sin\varepsilon$

$21^0 < \varepsilon < 180^0$: $C^*_T = 0.099 \cos\varepsilon|\cos\varepsilon| - 0.671 \sin\varepsilon|\sin\varepsilon|$

$10C^*_Q = 0.158 \cos\varepsilon|\cos\varepsilon| - 0.824 \sin\varepsilon|\sin\varepsilon|$

Interaction Factors:

$w_R \simeq w = 0.530$ (Model)
$w_R \simeq w = 0.370$ (Ship)
$t = 0.191$
$Y''_{PT+} = -0.030$ $N''_{PT+} = 0.015$
$Y''_{PT-} = 0.410$ $N''_{PT-} = -0.105$
$k_{HR} = 1.000$ $k_{PR} = 0.870$

Rudder Coefficients:

δ_e	C^0_{LR}	C^0_{DR}
0 deg	0.0000	0.0000
15 deg	0.2401	0.0428
30 deg	0.4539	0.1875
45 deg	0.5789	0.4250
50 deg	0.2960	0.3057
90 deg	0.0329	0.5096

$k_{LR} = 5.30$
$k_{DR} = 2.50$
$k_{NR} = 0.12$
$x''_R = -0.50$

Machinery Characteristics

Steering Gear:

$|\delta| < 40.0$ deg $\tau_L = 0.00$ s
$|\dot{\delta}| < 2.32$ deg/s

Turbine Torque:

$a = 0.075$ $A_f = 2.500$ $A_b = 1.000$
$b = 0.250$ $B_f = 1.000$ $B_b = 0.600$

Table 4

Computed zigzag maneuver characteristics of the tanker at an approach speed U_o = 15 kn

Top: Constant propeller rate, model condition
Bottom: Constant steam rate, ship condition

Rudder angle	Course change	Time to attain course change	Time to check yaw to starboard	Time for counterturn	Time to return to base course	Time to check yaw to port	Period of zigzag	Overswing to starboard	Overswing to port	Maximum transfer	Turning rate to starboard	Turning rate to port
δ_m	ψ_s	τ_a	τ_{b1}	τ_c	τ_r	τ_{b2}	T	α_{O1}	α_{O2}	$y_{o\,max}$	$\lvert r\rvert_{max1}$	$\lvert r\rvert_{max2}$
deg	deg	s	s	s	s	s	s	deg	deg	m	deg/s	deg/s
5.0	10.0	85.5	66.5	142.0	294.0	60.0		4.8	4.8	333.4	0.189	0.203
10.0	10.0	61.3	40.2	95.3	196.8	42.4	351.9	4.9	5.5	211.8	0.267	0.294
15.0	10.0	51.0	34.0	78.1	163.1	36.7	291.2	5.8	6.6	179.7	0.332	0.367
20.0	10.0	45.3	32.7	69.6	147.5	34.8	261.6	7.2	7.9	170.1	0.389	0.429
25.0	10.0	41.8	33.0	65.0	139.8	34.8	246.5	8.7	9.4	170.3	0.440	0.483
30.0	10.0	39.6	34.3	62.3	136.2	35.6	239.2	10.3	11.0	176.3	0.485	0.532
35.0	10.0	38.0	36.1	61.2	135.3	37.3	237.0	12.1	12.6	185.4	0.526	0.573
40.0	10.0	37.1	38.7	60.9	136.7	40.1	240.6	13.9	14.2	199.4	0.562	0.607
20.0	20.0	69.1	36.8	99.9	205.8	36.7	368.4	8.5	8.2	386.4	0.442	0.433
5.0	10.0	88.5	48.0	131.0	267.5	50.5		3.4	3.9	267.1	0.176	0.192
10.0	10.0	61.6	33.2	89.2	184.0	37.0	332.0	4.1	4.8	183.7	0.259	0.284
15.0	10.0	50.7	29.8	73.8	154.3	33.1	277.8	5.2	5.9	160.2	0.327	0.358
20.0	10.0	44.8	29.6	66.2	140.5	32.4	252.1	6.6	7.3	154.3	0.387	0.420
25.0	10.0	41.3	30.6	61.9	133.8	33.0	239.7	8.2	8.9	156.9	0.439	0.476
30.0	10.0	38.9	32.3	59.8	131.0	34.3	234.4	9.8	10.5	163.6	0.487	0.523
35.0	10.0	36.6	35.2	58.8	130.5	36.3	233.9	11.6	12.0	173.5	0.529	0.564
40.0	10.0	36.5	36.8	58.8	132.2	40.0	240.3	13.4	13.7	186.7	0.566	0.598
20.0	20.0	69.0	32.8	96.5	198.3	34.5	365.0	7.6	7.5	355.9	0.432	0.419

Table 5

Computed turning circle characteristics of the tanker at an approach speed U_o = 15 kn

Top: Constant propeller rate, model condition
Bottom: Constant steam rate, ship condition

Rudder angle δ	Advance x_o at ψ = 90°	Transfer y_o at ψ = 90°	Maximum advance	Tactical diameter	Time t at ψ = 90°	Time t at ψ = 180°	Maximum transfer	Final values in steady turn: Turning radius R	Drift angle β	Turning rate r	Track speed U	Speed ratio U/U_o
deg	m	m	m	m	s	s	m	m	deg	deg/s	kn	1
5.0	2603	-1835	2609	3864	478	898	-3870	1884	-4.48	-0.212	13.55	0.903
-5.0	2301	1598	2307	3382	421	793	3389	1625	5.15	0.239	13.18	0.879
10.0	1796	-1201	1804	-2595	330	632	-2603	1230	-6.75	-0.289	12.06	0.804
-10.0	1684	1113	1693	2410	309	591	2419	1123	7.37	0.307	11.70	0.780
15.0	1458	-928	1469	-2041	268	521	-2052	930	-8.81	-0.337	10.63	0.709
-15.0	1395	878	1406	1934	256	497	1946	863	9.48	0.351	10.28	0.685
20.0	1263	-766	1275	-1708	233	458	-1721	742	-10.93	-0.370	9.31	0.621
-20.0	1220	733	1233	1636	225	441	1649	691	11.69	0.383	8.98	0.599
25.0	1134	-655	1148	-1479	210	416	-1494	606	-13.17	-0.393	8.08	0.539
-25.0	1102	631	1117	1425	203	403	1440	565	14.07	0.406	7.78	0.519
30.0	1042	-574	1058	-1309	194	388	-1327	502	-15.62	-0.410	6.98	0.465
-30.0	1017	556	1033	1266	188	376	1285	468	16.70	0.422	6.70	0.447
35.0	973	-512	992	-1176	182	368	-1196	418	-18.38	-0.422	5.99	0.399
-35.0	953	497	970	1141	177	357	1162	388	19.69	0.435	5.73	0.382
40.0	921	-463	941	-1069	173	358	-1092	349	-21.63	-0.428	5.07	0.338
-40.0	903	450	923	1039	169	344	1063	322	23.30	0.444	4.85	0.323
5.0	2674	-1963	2679	-4126	500	957	-4132	2006	-4.20	-0.191	13.00	0.867
-5.0	2486	1804	2491	3796	463	887	3802	1814	4.62	0.206	12.68	0.845
10.0	1820	-1253	1828	-2700	340	664	-2708	1254	-6.64	-0.256	10.89	0.726
-10.0	1754	1197	1763	2579	327	638	2588	1172	7.10	0.266	10.58	0.705
15.0	1467	-956	1478	-2098	274	546	-2109	919	-8.98	-0.291	9.07	0.605
-15.0	1430	926	1441	2030	267	530	2042	867	9.53	0.299	8.79	0.586
20.0	1265	-783	1278	-1744	237	480	-1758	710	-11.42	-0.312	7.52	0.501
-20.0	1241	763	1253	1698	232	468	1712	671	12.09	0.320	7.28	0.485
25.0	1132	-667	1147	-1504	213	438	-1520	567	-14.08	-0.325	6.25	0.417
-25.0	1114	652	1129	1469	209	428	1486	530	14.95	0.335	6.02	0.401
30.0	1038	-582	1055	-1327	197	409	-1346	458	-17.00	-0.335	5.20	0.347
-30.0	1024	571	1041	1299	193	401	1319	429	18.05	0.345	5.02	0.335
35.0	968	-517	986	-1190	184	389	-1212	376	-20.30	-0.341	4.35	0.290
-35.0	956	508	975	1167	182	382	1189	352	21.60	0.352	4.20	0.280
40.0	915	-465	935	-1081	175	376	-1106	308	-24.12	-0.345	3.60	0.240
-40.0	904	458	925	1061	173	369	1087	288	25.80	0.356	3.48	0.232

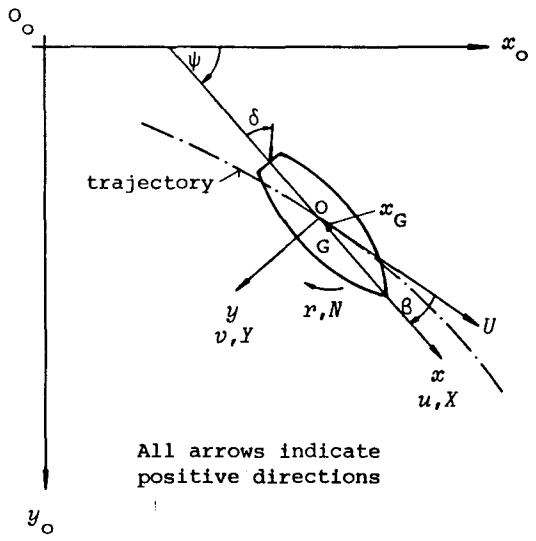

Fig. 1 Coordinate system

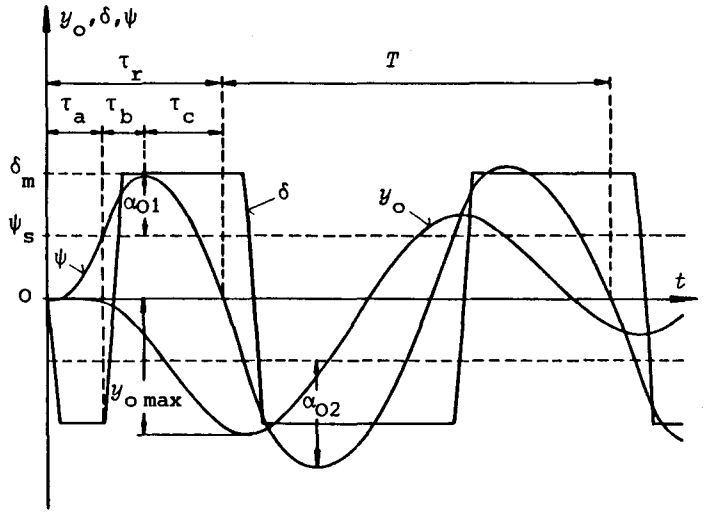

Fig. 2 Characteristic parameters of zigzag maneuver

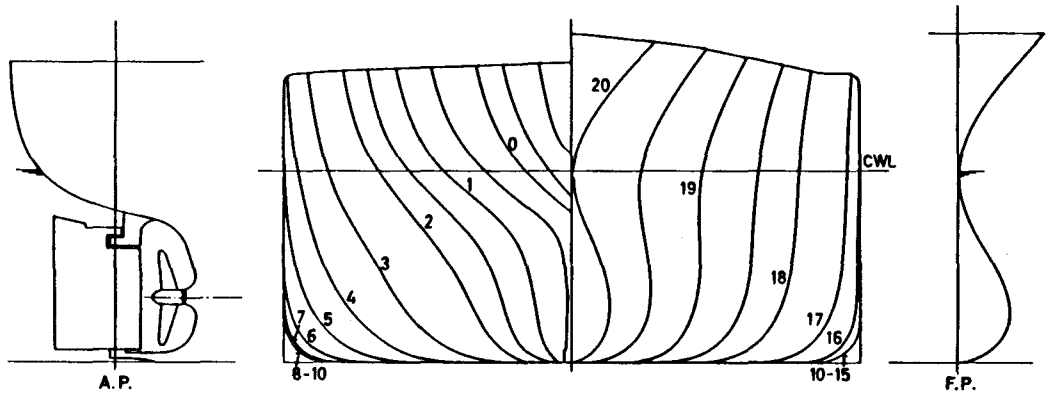

Fig. 3 Body plan and profile of tanker (HSVA Model 2507)

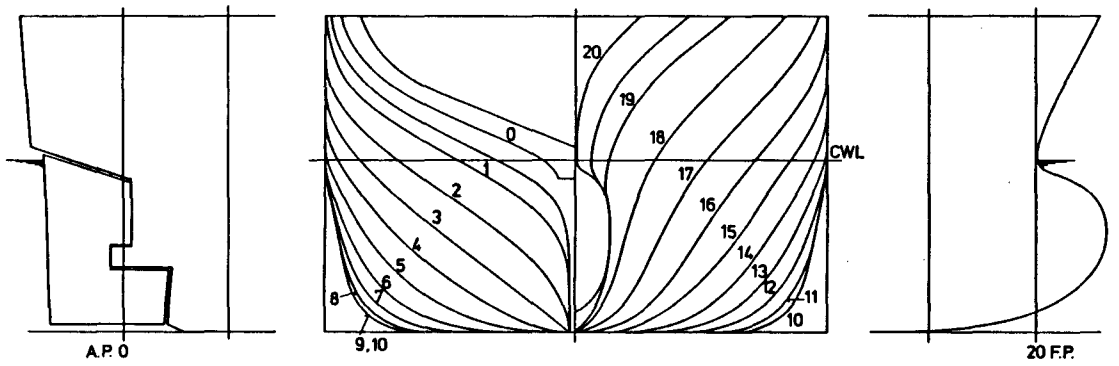

Fig. 4 Body plan and profile of container carrier (HSVA Model 2657)

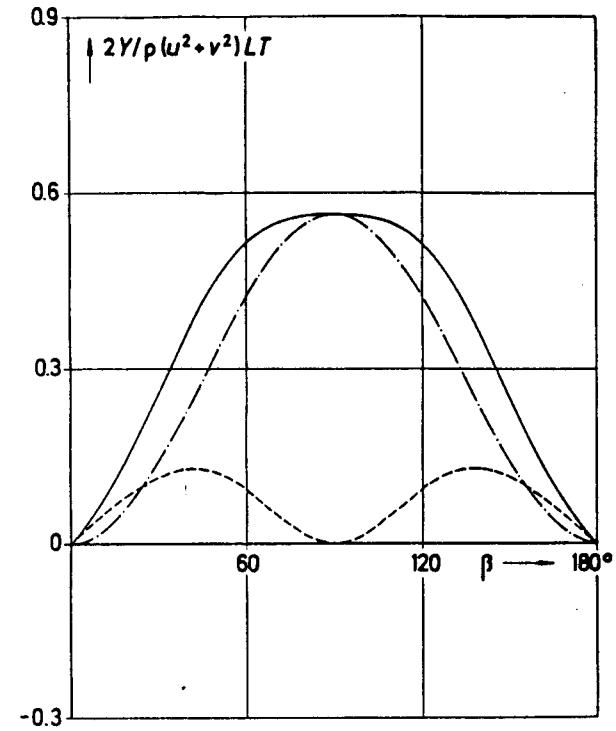

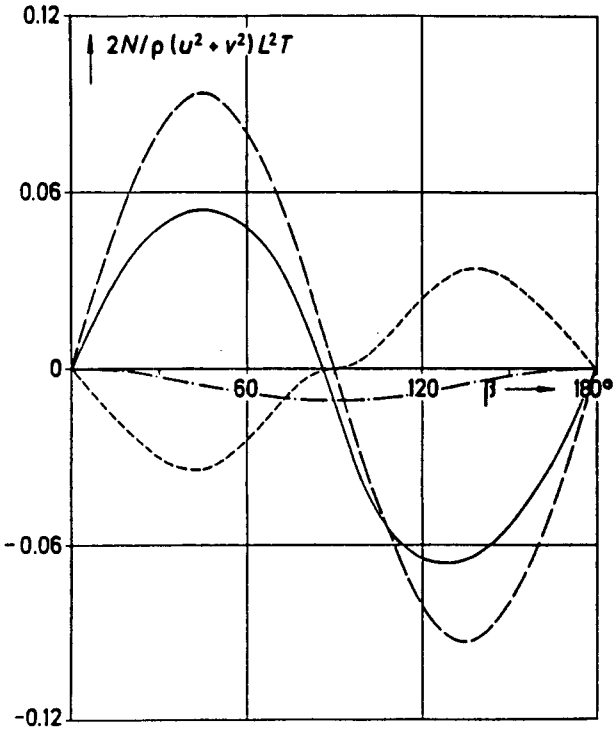

Fig. 5 Side force (top) and yaw moment (bottom) on the tanker resulting from pure drift

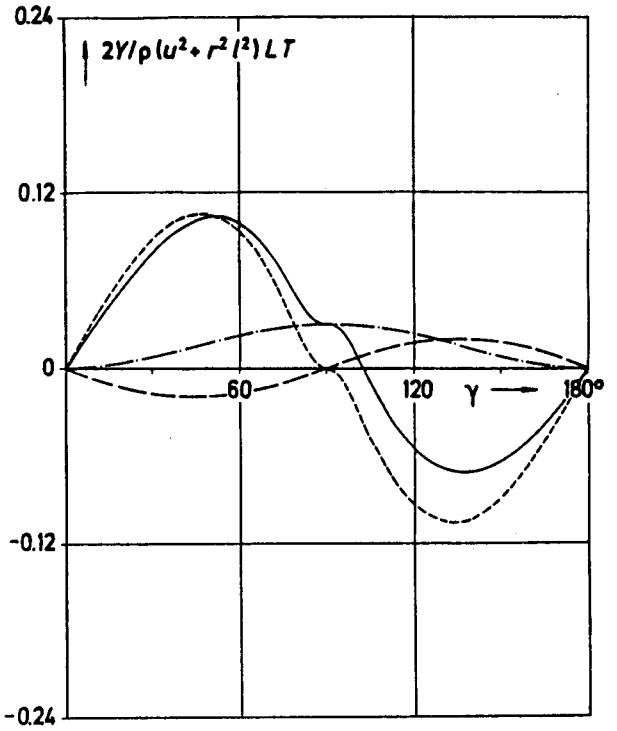

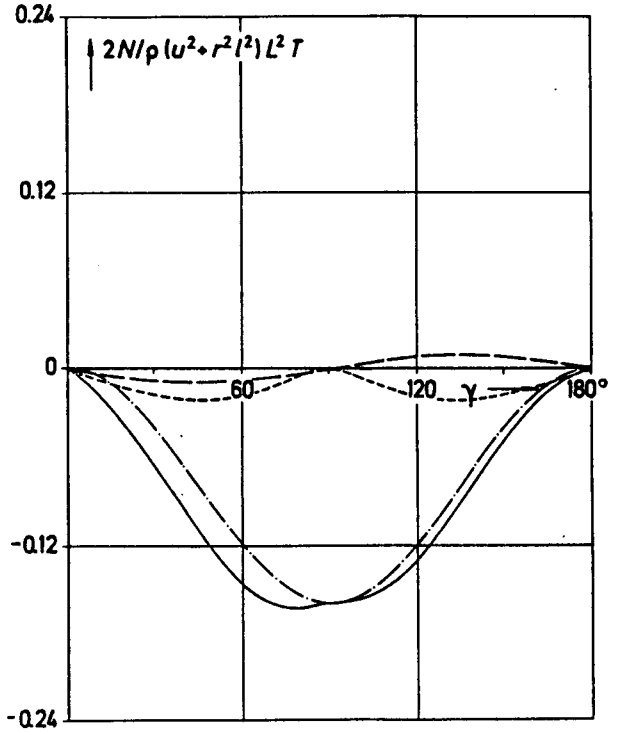

Fig. 6 Side force (top) and yaw moment (bottom) on the tanker resulting from pure yaw

Common legend
— — — Ideal fluid effects
- - - - - - - - Lifting effects
—·—·— Cross flow effects
———— Total

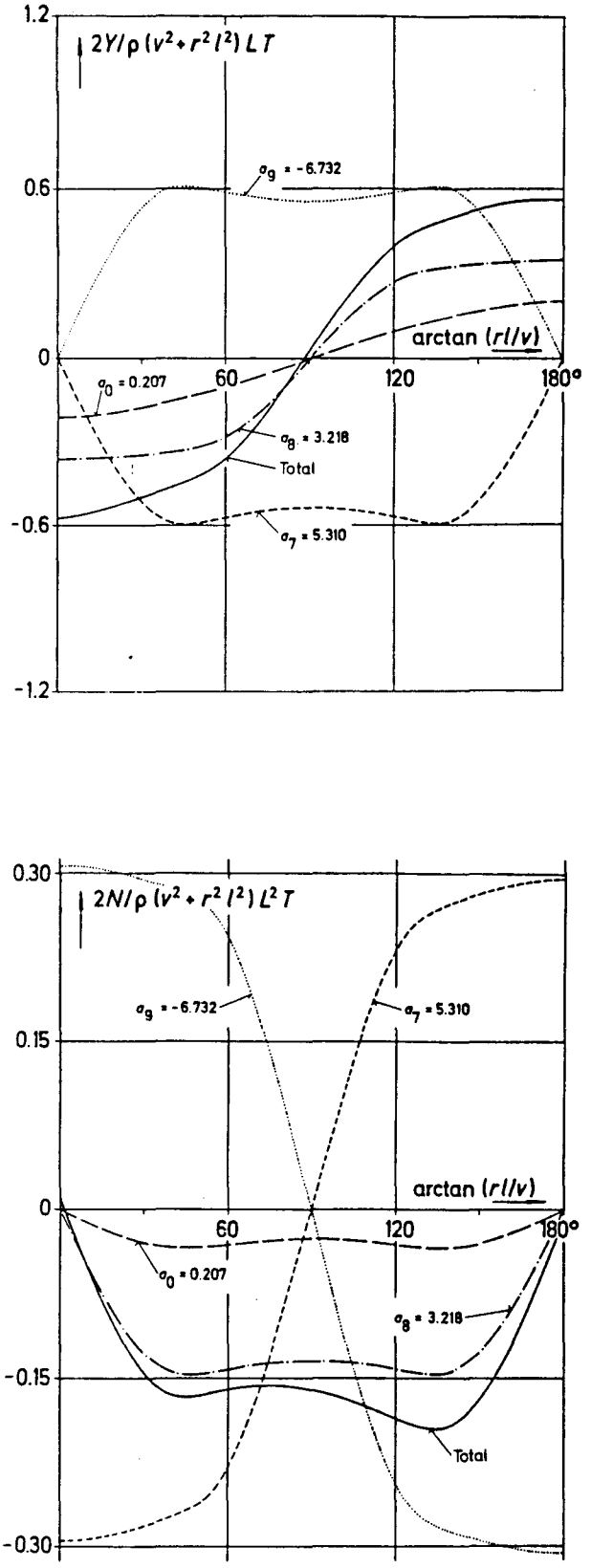

Fig. 7 Side force (top) and yaw moment (bottom) on the tanker resulting from pure cross flow as measured at zero forward speed

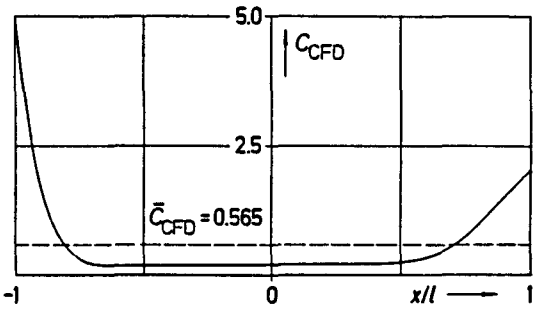

Fig. 8 Local drag coefficient associated with observed cross flow effects on tanker

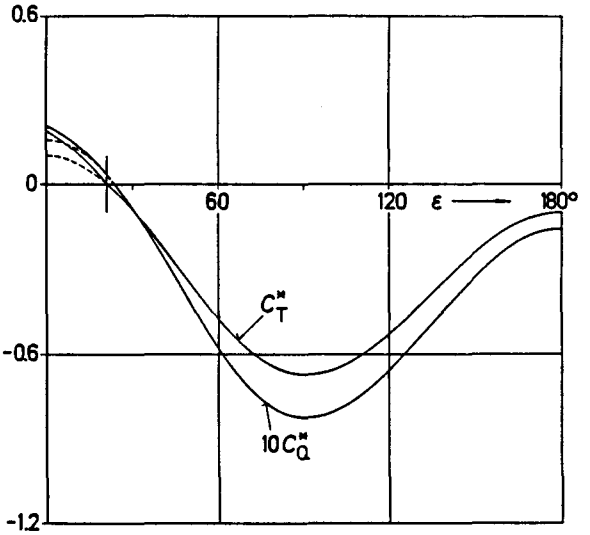

Fig. 9 Thrust and torque characteristics of the tanker propeller

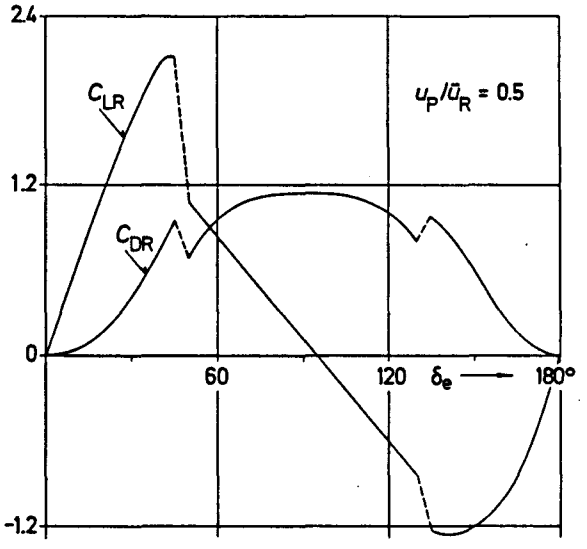

Fig. 10 Lift and drag characteristics of the tanker rudder

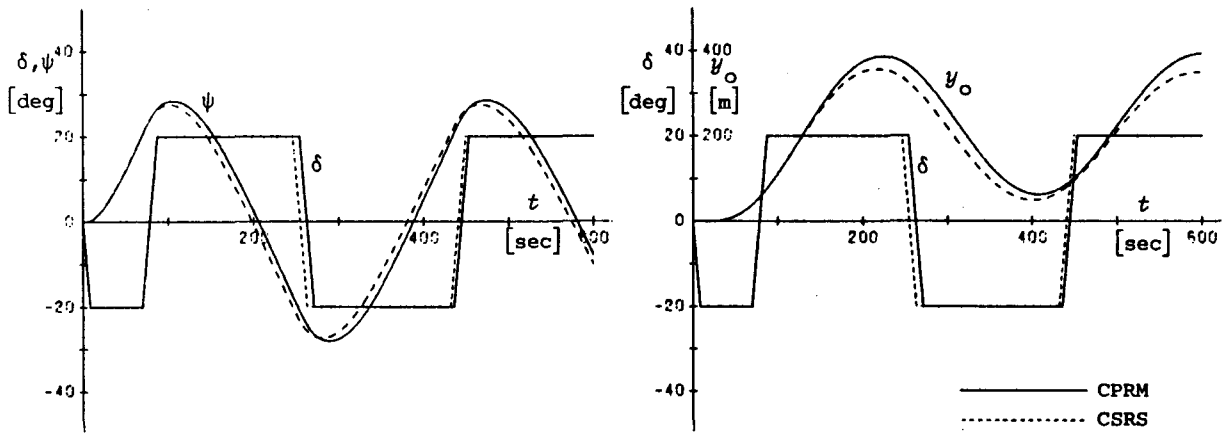

Fig. 11 Simulated $20^o/20^o$ zigzag maneuver of the tanker (CPRM versus CSRS)

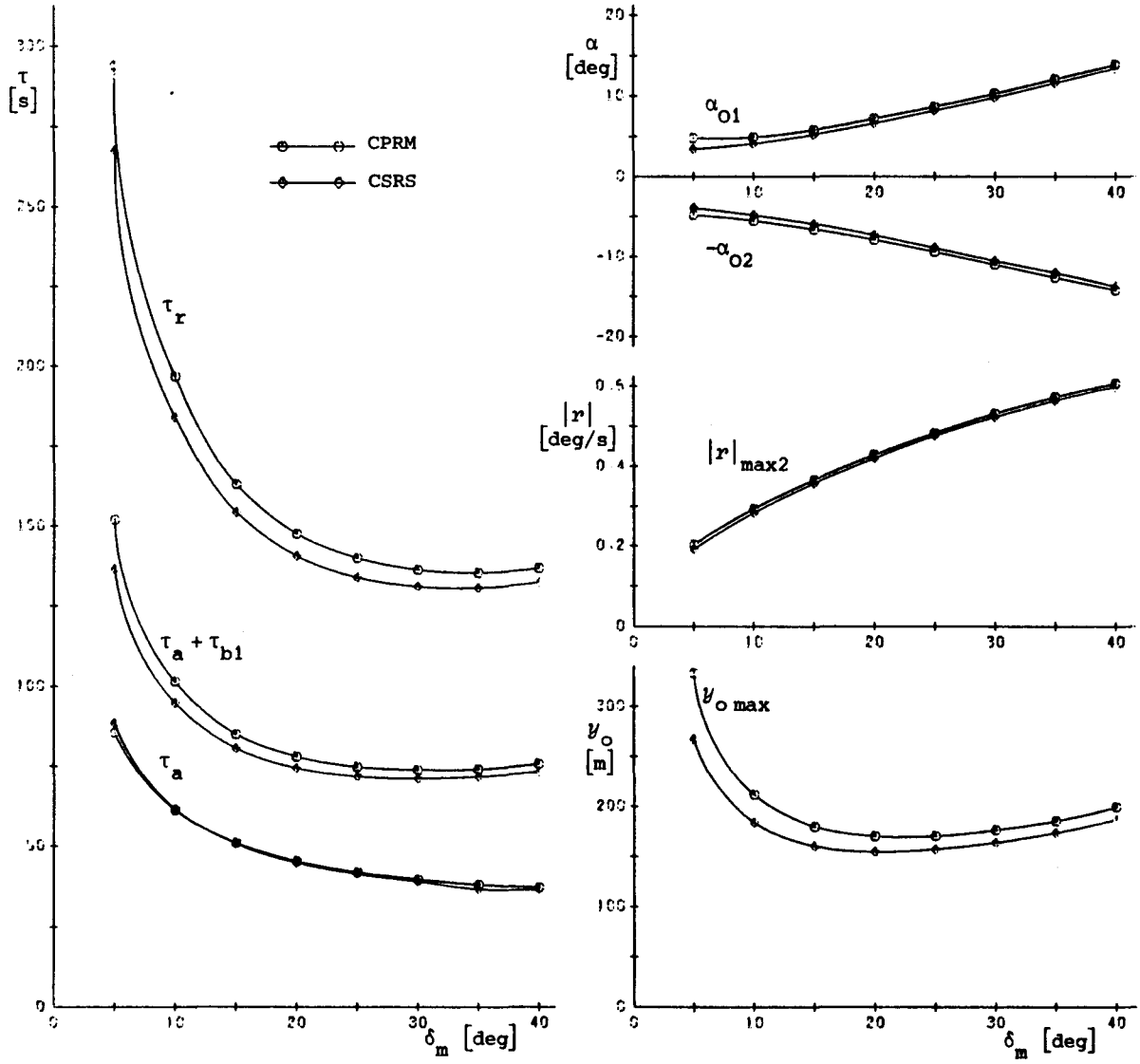

Fig. 12 Selected zigzag maneuver characteristics of the tanker (CPRM versus CSRS)

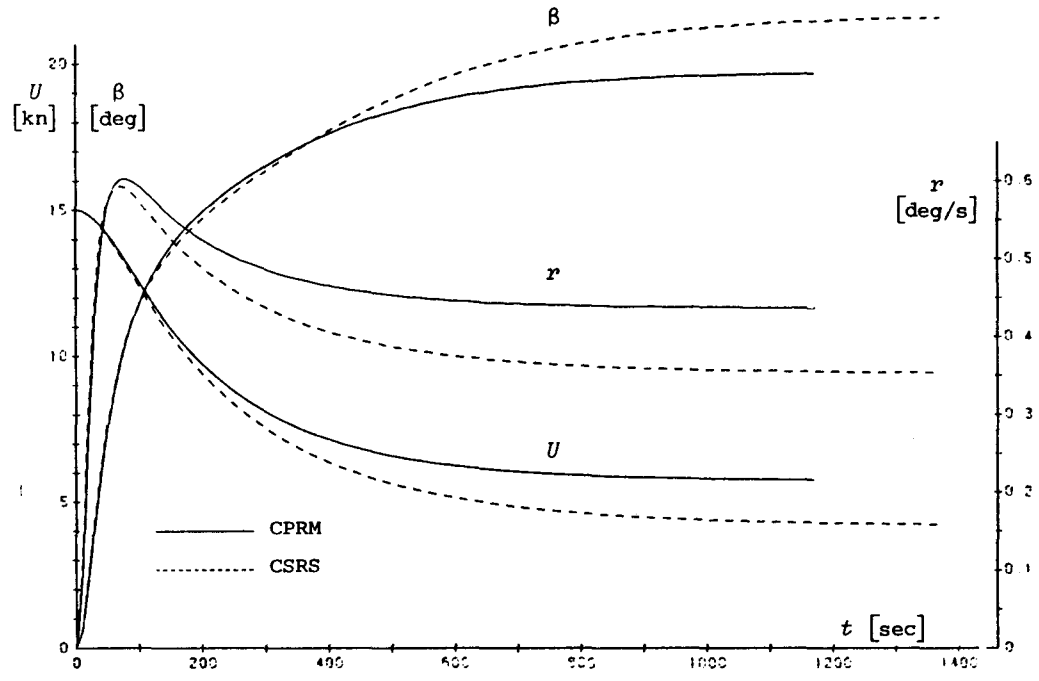

Fig. 13 Simulated turning circle (δ = -35^{o}) maneuver of the tanker (CPRM versus CSRS)

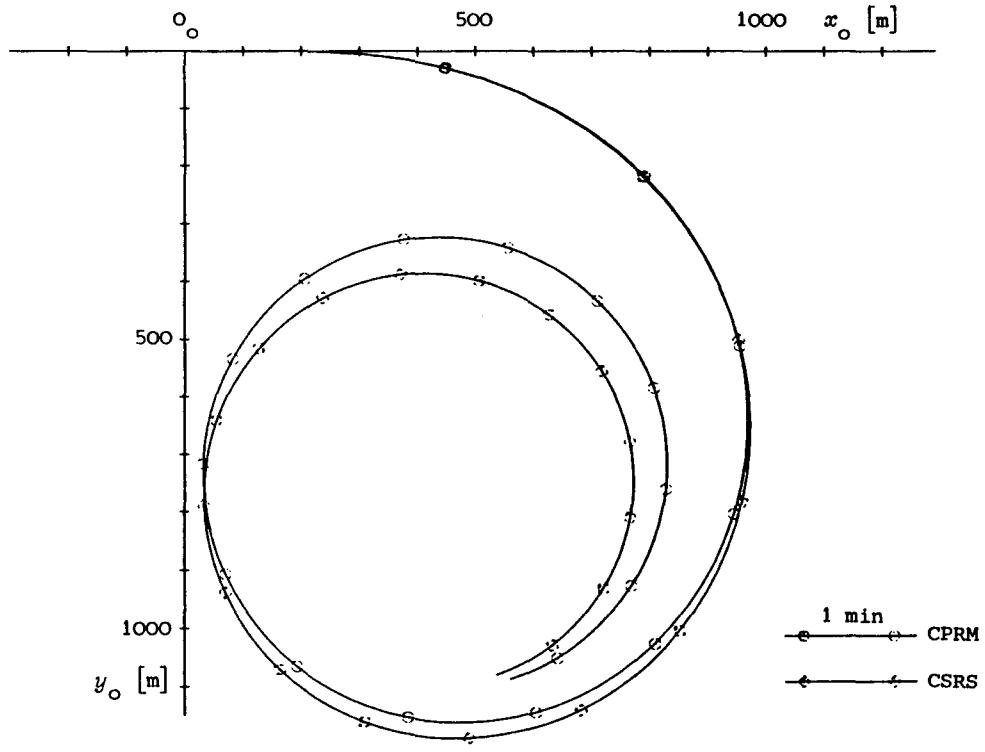

Fig. 14 Simulated turning circle (δ = -35^{o}) trajectory of the tanker (CPRM versus CSRS)

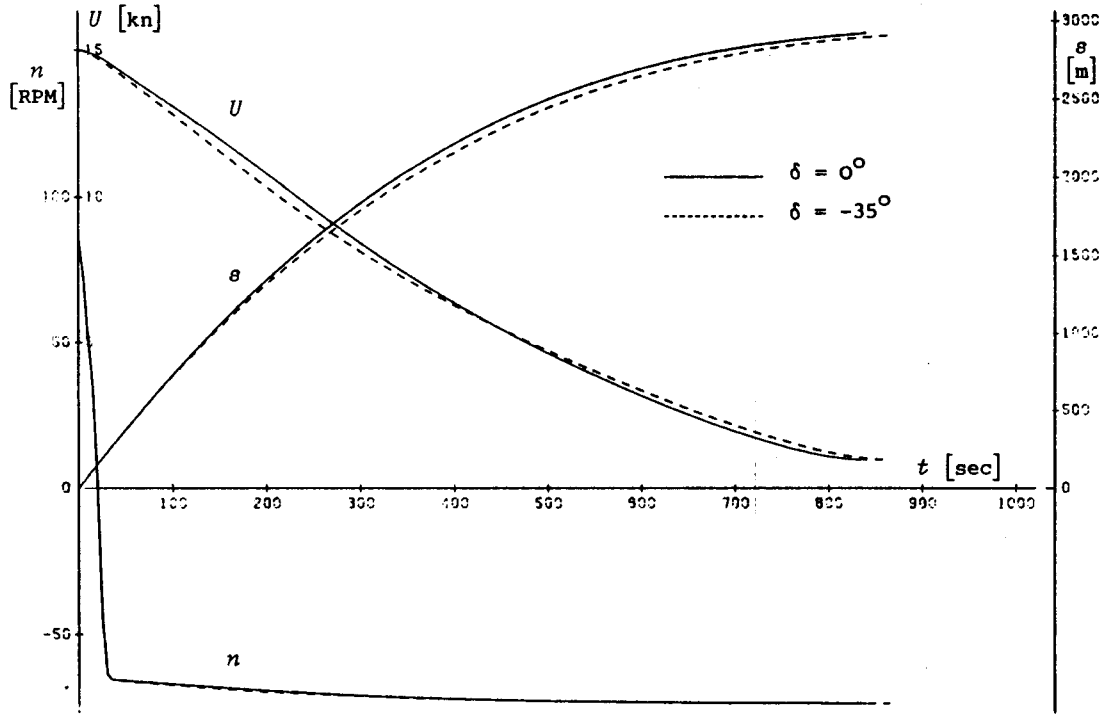

Fig. 15 Simulated crashback maneuvers of the tanker with and without rudder application

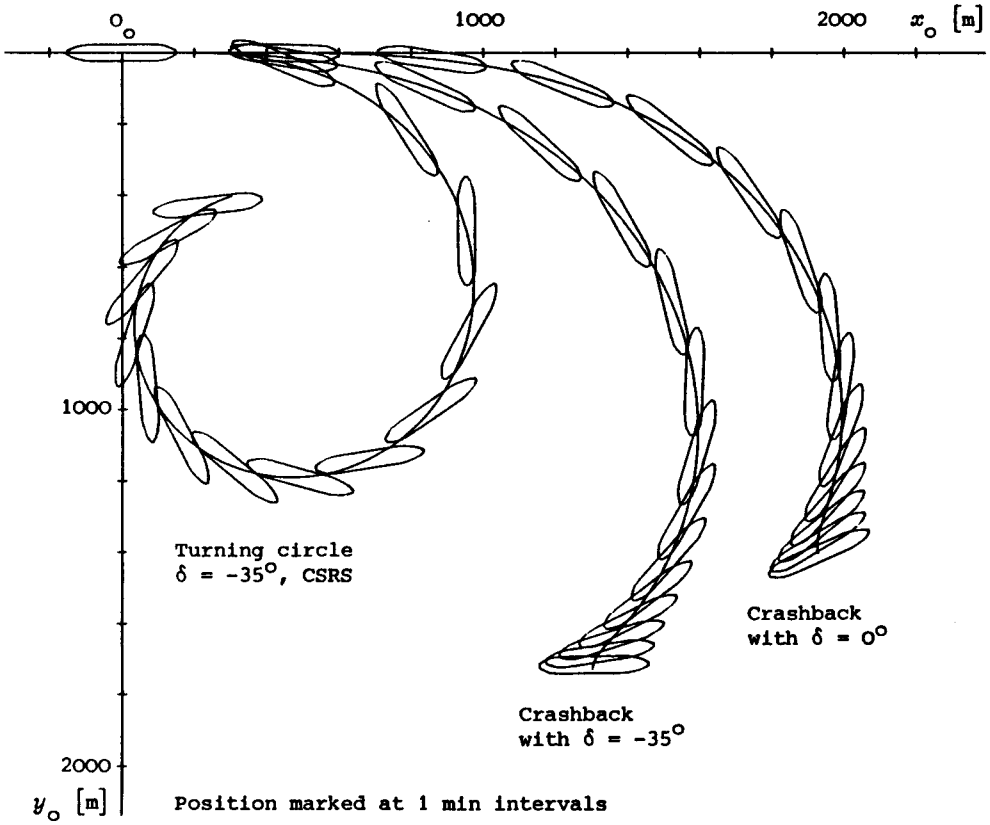

Fig. 16 Comparison of crashback and turning circle trajectories for the tanker

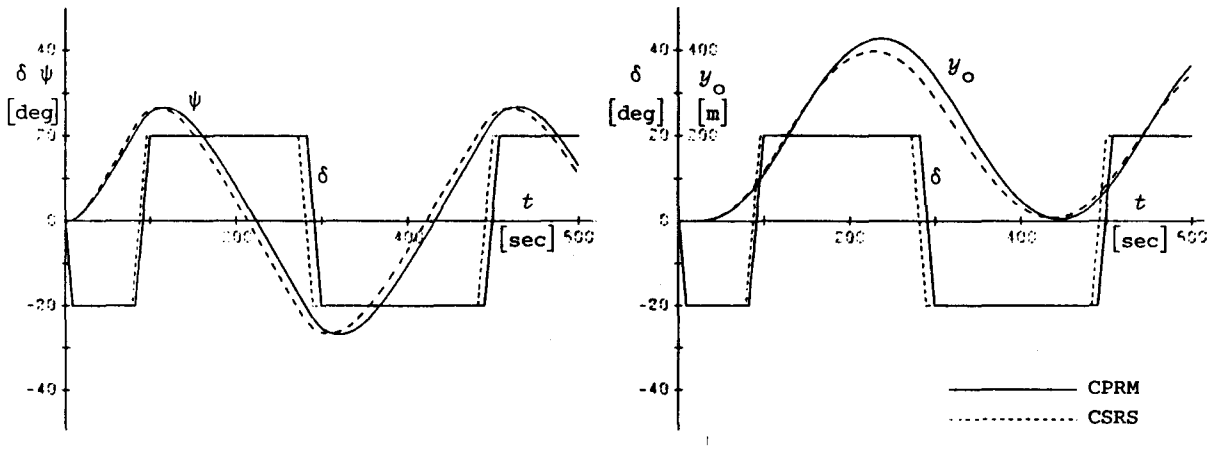

Fig. 17 Simulated $20^0/20^0$ zigzag maneuver of the container carrier (CPRM versus CSRS)

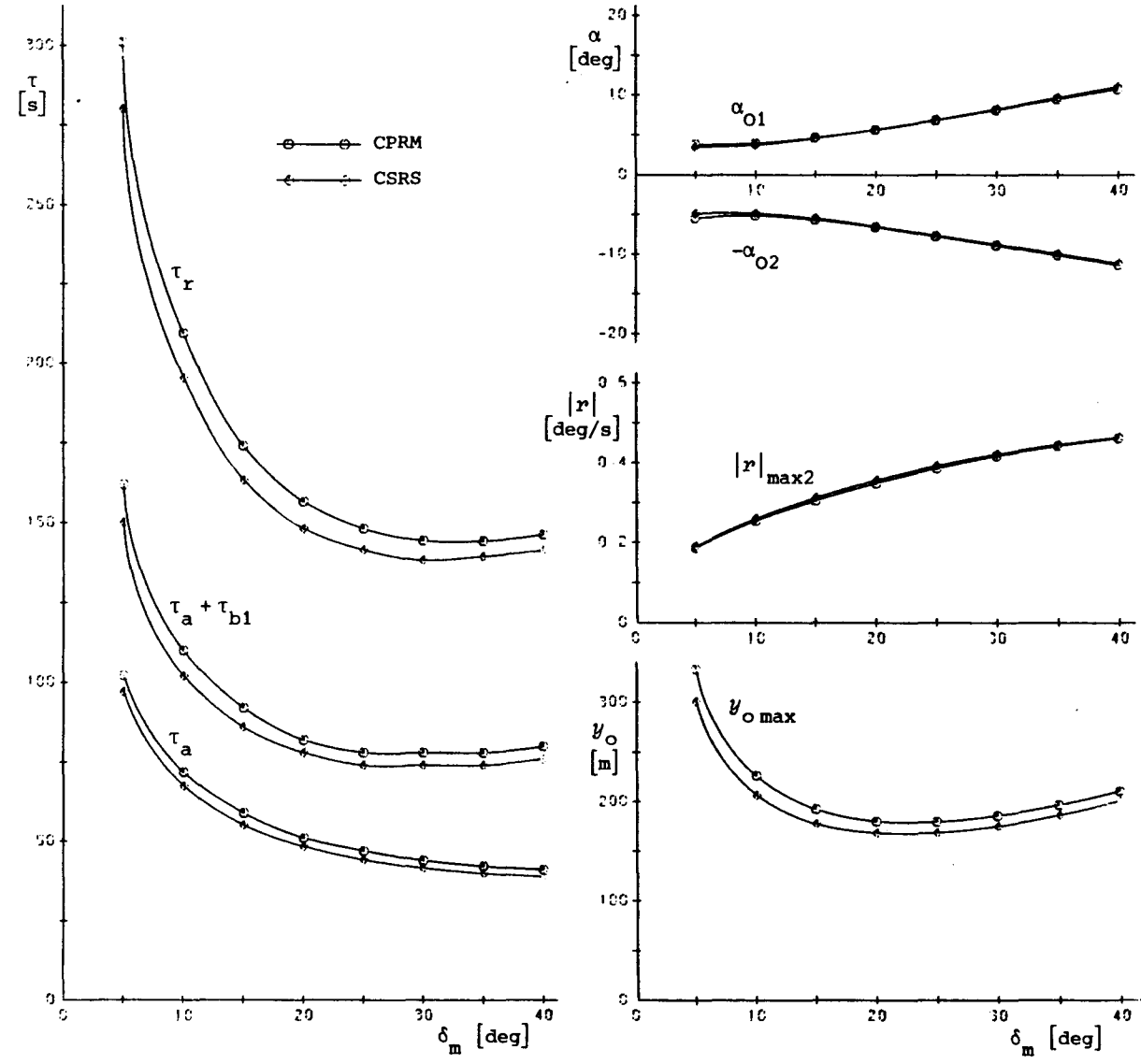

Fig. 18 Selected zigzag maneuver characteristics of the container carrier (CPRM versus CSRS)

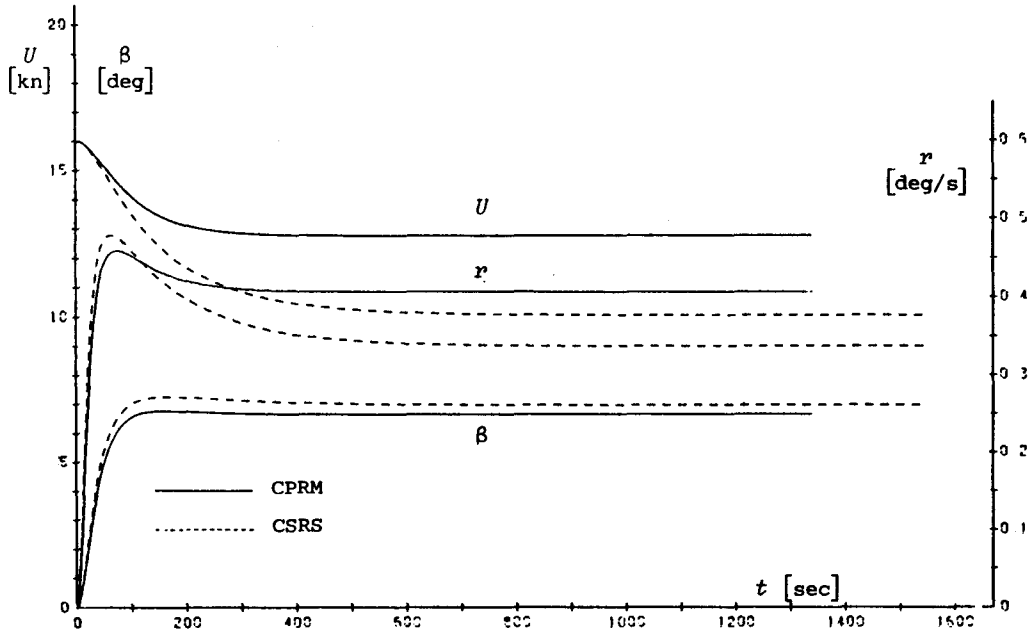

Fig. 19 Simulated turning circle (δ = -35°) maneuver of the container carrier (CPRM versus CSRS)

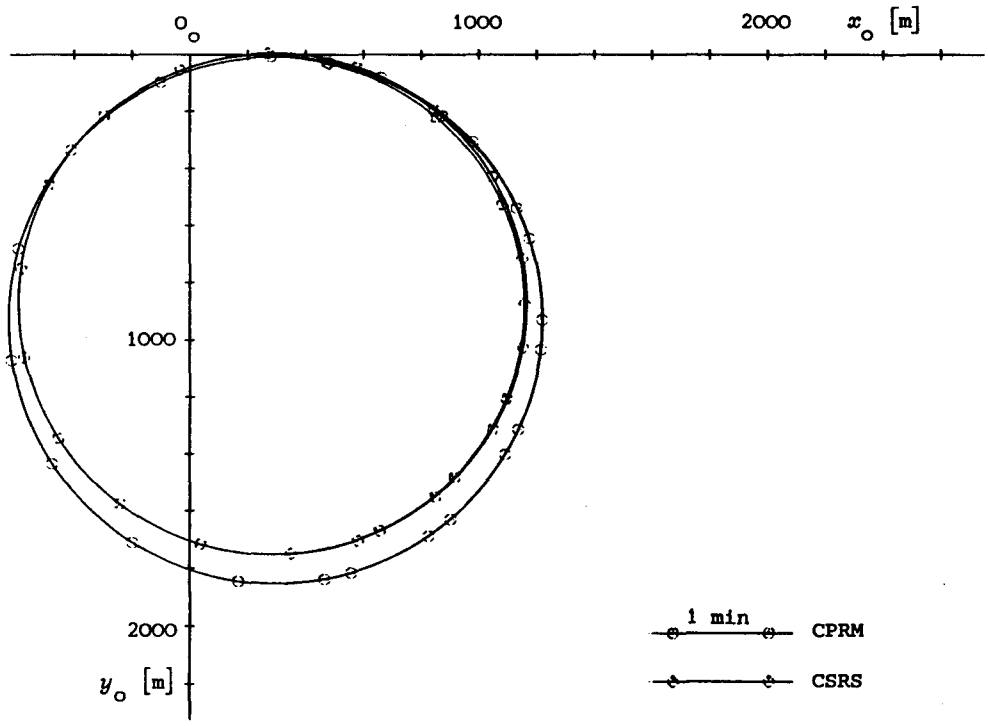

Fig. 20 Simulated turning circle (δ = -35°) trajectory of the container carrier (CPRM versus CSRS)

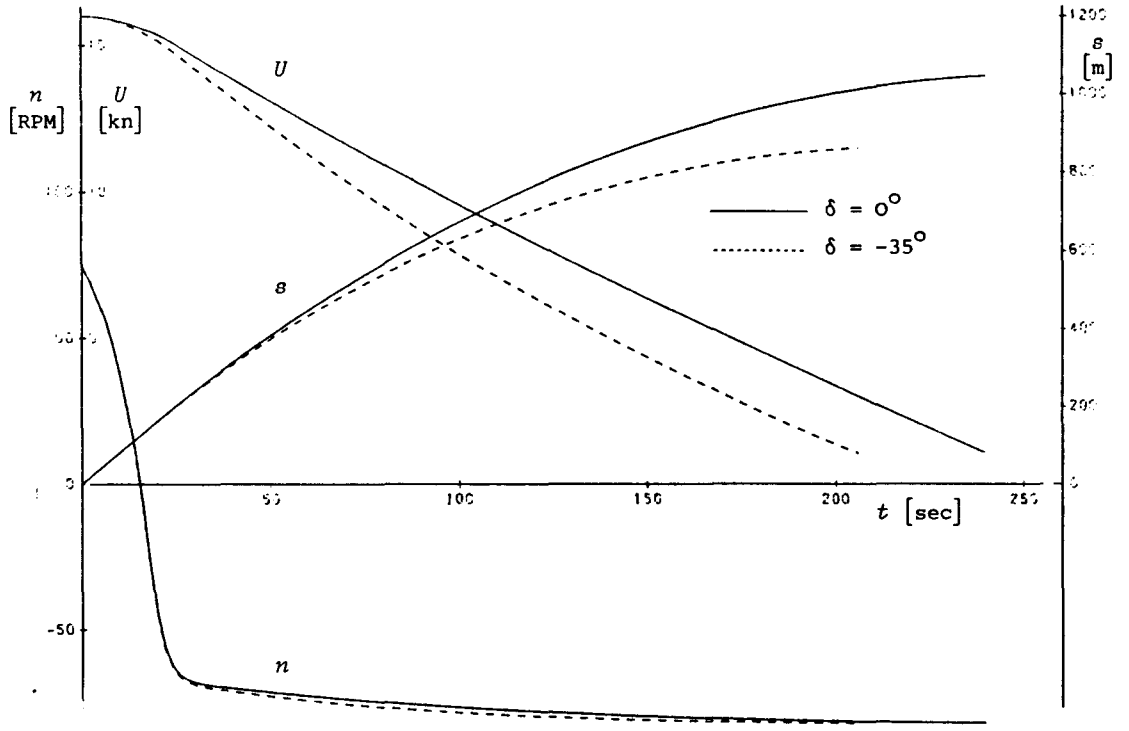

Fig. 21 Simulated crashback maneuvers of the container carrier with and without rudder application

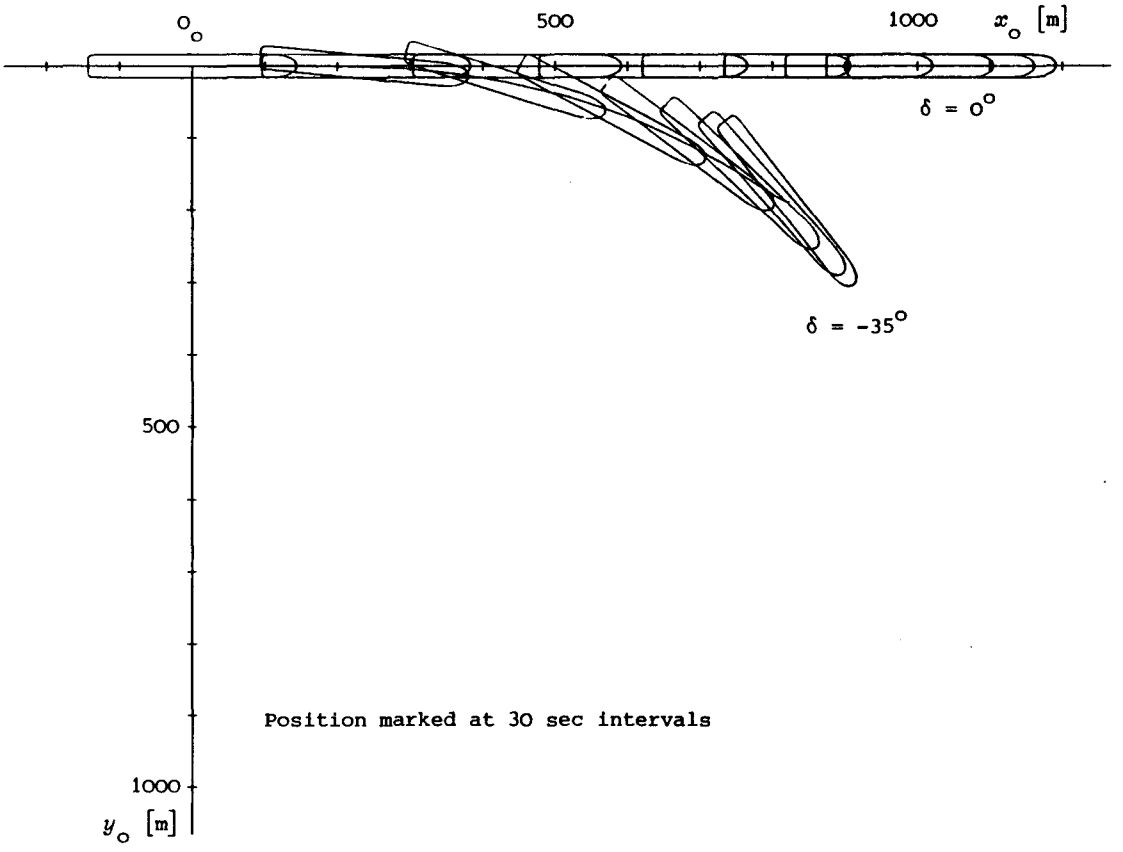

Fig. 22 Simulated crashback trajectories of the container carrier with and without rudder application

ADDENDUM

The integral occurring in Section 2.2.4. Hull Cross-Flow Effects has the following general solution:

$$\int_{-l}^{l} x^n (v + rx) \, |v + rx| \, dx = 2l^{n+1} \left\{ \frac{v^2}{n+1} + \frac{r^2 l^2}{n+3} \right\} \operatorname{sgn} v \qquad [v^2 > r^2 l^2, \; n \text{ even}]$$

$$= \frac{4l^{n+1}}{n+2} \, vrl \, \operatorname{sgn} v \qquad [v^2 > r^2 l^2, \; n \text{ odd}]$$

$$= \frac{4l^{n+1}}{n+2} \left\{ rl + \frac{v^{n+2}}{(n+1)(n+3)(rl)^{n+1}} \right\} v \operatorname{sgn} r \qquad [v^2 < r^2 l^2, \; n \text{ even}]$$

$$= l^{n+1} \left\{ \frac{2v^2}{n+1} + \frac{2r^2 l^2}{n+3} - \frac{4v^{n+3}}{(n+1)(n+2)(n+3)(rl)^{n+1}} \right\} \operatorname{sgn} r \qquad [v^2 < r^2 l^2, \; n \text{ odd}]$$

Substitution of Eq. (34-35) into Eq. (32-33) then yields the following specific expressions for side force and yaw moment in response to cross flow:

$$Y_{HC} = -\frac{\rho}{2} LT \left\{ a_0 \left(v^2 + \frac{r^2 l^2}{3} \right) + a_7 \frac{2}{9} vrl + a_8 \left(\frac{v^2}{9} + \frac{r^2 l^2}{11} \right) + a_9 \frac{2}{11} vrl \right\} \operatorname{sgn} v \qquad [v^2 > r^2 l^2]$$

$$= -\frac{\rho}{2} LT \left\{ a_0 \left(rl + \frac{v^2}{3rl} \right) v + a_7 \frac{1}{2} \left(\frac{v^2}{4} + \frac{r^2 l^2}{5} - \frac{v^{10}}{180 r^8 l^8} \right) \right.$$

$$\left. + a_8 \frac{1}{5} \left(rl + \frac{v^{10}}{99 r^9 l^9} \right) v + a_9 \frac{1}{2} \left(\frac{v^2}{5} + \frac{r^2 l^2}{6} - \frac{v^{12}}{330 r^{10} l^{10}} \right) \right\} \operatorname{sgn} r \qquad [v^2 < r^2 l^2]$$

$$N_{HC} = -\frac{\rho}{2} L^2 T \left\{ a_0 \frac{1}{3} vrl + a_7 \frac{1}{2} \left(\frac{v^2}{9} + \frac{r^2 l^2}{11} \right) + a_8 \frac{1}{11} vrl + a_9 \frac{1}{2} \left(\frac{v^2}{11} + \frac{r^2 l^2}{13} \right) \right\} \operatorname{sgn} v \qquad [v^2 > r^2 l^2]$$

$$= -\frac{\rho}{2} L^2 T \left\{ a_0 \frac{1}{4} \left(v^2 + \frac{r^2 l^2}{2} - \frac{v^4}{6 r^2 l^2} \right) + a_7 \frac{1}{10} \left(rl + \frac{v^{10}}{99 r^9 l^9} \right) v \right.$$

$$\left. + a_8 \frac{1}{4} \left(\frac{v^2}{5} + \frac{r^2 l^2}{6} - \frac{v^{12}}{330 r^{10} l^{10}} \right) + a_9 \frac{1}{12} \left(rl + \frac{v^{12}}{143 r^{11} l^{11}} \right) v \right\} \operatorname{sgn} r \qquad [v^2 < r^2 l^2]$$

Our simulation algorithm actually uses these analytical formulas, but numerical quadrature would be an equally admissible alternative.